Michigan Technological University
Create the Future Digital Commons @ Michigan Tech

Dissertations, Master's Theses and Master's Reports - Open

Dissertations, Master's Theses and Master's Reports

2013

Maximum principle preserving high order schemes for convection-dominated diffusion equations

Yi Jiang
Michigan Technological University

Follow this and additional works at: https://digitalcommons.mtu.edu/etds

 Part of the Mathematics Commons

Copyright 2013 Yi Jiang

Recommended Citation

Jiang, Yi, "Maximum principle preserving high order schemes for convection-dominated diffusion equations", Master's Thesis, Michigan Technological University, 2013.
https://doi.org/10.37099/mtu.dc.etds/594

Follow this and additional works at: https://digitalcommons.mtu.edu/etds

 Part of the Mathematics Commons

MAXIMUM PRINCIPLE PRESERVING HIGH ORDER SCHEMES FOR CONVECTION-DOMINATED DIFFUSION EQUATIONS

By

Yi Jiang

A THESIS

Submitted in partial fulfillment of the requirements for the degree of

MASTER OF SCIENCE

In Mathematical Sciences

MICHIGAN TECHNOLOGICAL UNIVERSITY

2013

© 2013 Yi Jiang

This thesis has been approved in partial fulfillment of the requirements for the Degree of MASTER OF SCIENCE in Mathematical Sciences.

Department of Mathematical Sciences

Thesis Advisor: Dr. *Zhengfu Xu*

Committee Member: Dr. *Allan A. Struthers*

Committee Member: Dr. *Song-Lin Yang*

Department Chair: Dr. *Mark S. Gockenbach*

Contents

[1] The material contained in this chapter has been submitted for publication.
[2] The material contained in this chapter has been submitted for publication.
[3] The material contained in this chapter has been submitted for publication.

List of Figures

List of Tables

Preface

Several chapters (Chapter 4, 5, 6) in this thesis are contained in the paper *Parametrized maximum principle preserving limiter for finite difference WENO schemes solving convection-dominated diffusion equations*. This is a joint work with Dr. Zhengfu Xu. The author performed the research and wrote the paper, except for the introduction part, with the guidance and editing provided by Dr. Zhengfu Xu. Some minor editorial changes are made concerning the whole picture of the thesis's topic. The paper has been recently submitted for publication.

Acknowledgments

My sincere appreciation goes to my advisor, Dr. Zhengfu Xu. It was his teaching in Numerical PDE that started my exploration in this interesting area. During the past year of research, I was deeply impressed by his broad knowledge and serious working attitude, and I'm so grateful that he was always being open for questions. Without his insightful suggestions, constant patience and warm encouragement, this thesis would never have been possible. I'm looking forward to our further collaborations very much.

I would also like to extend my appreciation to Dr. Allan Struthers and Dr. Song-Lin Yang, who served as my committee members, for providing constructive feedbacks to my thesis and research work.

I'm indebted to all my professors and colleagues in Math Department. Special thanks to Ann Humes, Philip Kendall and Todd King, for offering valuable suggestions and sharing their experiences in undergraduate teaching. Also, many thanks go to Jeanne, Tori and Margaret for their warm help during my past two-year graduate study.

At last, I'd like to express my gratitudes to my beloved family and friends for their tremendous support and endless love. And Keguo, my husband, thanks for sharing the life with me for the past, the present and the future. You're the gift from God.

Abstract

The maximum principle is an important property of solutions to PDE. Correspondingly, it's of great interest for people to design a high order numerical scheme solving PDE with this property maintained. In this thesis, our particular interest is solving convection-dominated diffusion equation. We first review a nonconventional maximum principle preserving(MPP) high order finite volume(FV) WENO scheme, and then propose a new parametrized MPP high order finite difference(FD) WENO framework, which is generalized from the one solving hyperbolic conservation laws. A formal analysis is presented to show that a third order finite difference scheme with this parametrized MPP flux limiters maintains the third order accuracy without extra CFL constraint when the low order monotone flux is chosen appropriately. Numerical tests in both one and two dimensional cases are performed on the simulation of the incompressible Navier-Stokes equations in vorticity stream-function formulation and several other problems to show the effectiveness of the proposed method.

Keywords: Parametrized flux limiters, Maximum principle, High order, Finite volume, Finite difference method, ENO/WENO, Convection diffusion equation, TVD Runge-Kutta method, Incompressible Navier-Stokes equation

Chapter 1

Introduction

Convection-diffusion equation describes physical phenomena where the energy or other physical quantities are transferred inside a physical system due to two processes: diffusion and convection. The general form of nonlinear convection-diffusion equations in one dimension could be taken as following:

$$u_t + f(u)_x = A(u)_{xx}, \quad u(x,0) = u_0(x). \tag{1.1}$$

In the case of $A'(u) > 0$, the exact solution to (1.1) satisfies a strict maximum principle, that

$$u(x,t) \in [u_m, u_M], \quad t > 0$$

if

$$u_M = \max_x u_0(x), \qquad u_m = \min_x u_0(x). \tag{1.2}$$

Our particular interest is solving (1.1) when the problem is convection-dominated, which is a typical feature of flow problems such as incompressible Navier-Stokes equation with large Renolds number. The goal of our research is to explore high order numerical schemes solving convection-dominated equations while maintaining the discrete maximum principle(DMP):

$$u(x_j, t^n) \in [u_m, u_M], \tag{1.3}$$

for any j and n.

The maximum principle is an important property of solutions to partial differential equations(PDEs), of the elliptic and parabolic type. It is also a typical of the phenomenon the PDE usually simulates. Hence, it is natural to expect that numerical solutions could maintain the discrete equivalent of this property of exact solution. The earliest discussion of the DMP for parabolic equations can be traced back to Fujii [5], where linear element solution was investigated and, based on a triangulation of acute type, sufficient conditions were established for the finite element framework to possess the DMP. Recent developments can be found in [2, 3, 30] and references therein. [3] investigated sufficient conditions of DMP for nonlinear parabolic systems of PDE. In [30], sufficient conditions were derived for finite element method with discretization on right triangular prisms. For convection-dominated problem, the related early work can be found in [20], where a new conservative Petrov-Galerkin method was presented to achieve DMP. However, these methods are algebraic, dependent on the mesh geometry, and difficult to generalize to arbitrarily high order accurate methods.

For the convection-dominated diffusion problem, the solution exhibits the nature of the hyperbolic problem where $A(u) = 0$. Explicit time integration is proven to be sufficient as for the evolution of the numerical solution. Conventional mechanism for designing a stable numerical method with high resolution for pure convection

problem still applies: up-winding biased numerical fluxes, essentially non-oscillatory high order polynomial reconstruction for high order accuracy and stability etc. For the pure convection problem, we refer to the review paper by Shu [27] and the references therein for comprehensive discussion of the high order (Weighted) Essentially Non-Oscillatory(ENO/WENO) methods and implementation details. A brief introduction on this topic will also be given later in the thesis. For the diffusive term in the equation (1.1), high order central difference is generally used to produce accurate approximation. Then, for the time discretization, total variation diminishing (TVD) [28] or strong stability preserving (SSP) [6] Runge-Kutta(RK) method is very often applied to obtain high order accuracy.

However, regular high order ENO/WENO method solving the convection-dominated diffusion problem (1.1) generally produces numerical solution which overshoots or undershoots the theoretical upper or lower bound of the exact solution. Within the finite volume(FV) high order WENO framework [35], the authors generalized the maximum-principle-preserving(MPP) polynomial rescaling technique for pure convection problem [36] to the convection diffusion problem (1.1) to achieve the DMP with proven arbitrary high order accuracy regardless of number of dimensions. The generalization is based on a twice-integrated FV formulation of (1.1). The application of the polynomial rescaling suffers mainly from the CFL restriction and the complexity of the implementation. It is neither clear how the polynomial rescaling technique can be applied to the high order finite difference(FD) RK WENO schemes solving (1.1) to preserve maximum principle without sacrificing high order accuracy. The polynomial rescaling was also applied to a discontinuous Galerkin finite element method on triangular mesh to obtain the DMP [41], however only up to second order.

In this thesis, we provide a general framework for conservative high order schemes, exemplified by high order FD WENO methods with explicit RK time discretization to achieve the DMP by utilizing the parametrized MPP flux limiting technique developed by

Xu [33] for solving the hyperbolic problem

$$u_t + f(u)_x = 0, \quad u(x,0) = u_0(x). \tag{1.4}$$

The parametrized MPP flux limiting method for two-dimensional scalar problem was developed later in [15]. It was further generalized to high order RK WENO methods solving (1.4) and incompressible flow by Xiong et al. [32], where instead of applying flux limiters to each of the intermediate stage of the multi-stage RK temporal integration, the authors apply the MPP flux limiters to the overall numerical integral form of the high order numerical fluxes. To continue on this line of research, we will adopt the more general parametrized MPP flux limiting method in [32] to solve (1.1) and the corresponding multi-dimensional problem within the conservative high order FD RK WENO framework.

The proposed approach includes the following steps: First, a first order monotone scheme which preserves maximum principle is chosen for the later use of parametrized flux limiting; Second, high order FD RK WENO schemes shall be designed for the problem (1.1) in a conservative form; Finally the general parametrized flux limiting developed in [33, 15, 32] will be applied. Details of the implementation procedure shall be given later in the thesis. The proposed approach has several advantages. One is that it does not require reprocessing the reconstructed polynomials, but instead operates directly on the high order numerical fluxes, precisely the temporal integral of the numerical fluxes. The complexity of implementation is significantly reduced compared with the MPP finite volume WENO method presented in [35]. Another advantage is that this new parametrized flux limiters are less demanding on the CFL to maintain the MPP property with high order accuracy.

However, the proof given in this thesis is only for third order scheme. For arbitrarily high order scheme, the analysis becomes more difficult since our proof relies on Taylor expansion. In [35], the proof there is given for universal high order finite volume scheme within the proposed double-integral formulation in order to achieve maximum principle

and high order accuracy. Our proof is similar to those given in [32] for pure convection problem, relying on Taylor polynomial expansion. However, the analysis we are giving also differs from the proof in [32], where characteristic information is used in temporal direction. In our case, we rely on Taylor expansion in both temporal and spatial direction with the help of the PDE.

The generalization of the parametrized MPP flux limiters to the regular high order finite volume WENO scheme solving the convection-dominated problem shall be straightforward. However, we will focus on the high order finite difference WENO formulation in this thesis.

The thesis is organized as follows. In Chapter 2, we'll give a brief introduction on ENO and WENO reconstruction in one dimensional case, where both the finite volume and finite difference method will be investigated. In Chapter 3, a nonconventional MPP high order FV WENO scheme will be reviewed. In Chapter 4, we will briefly introduce the high order FD RK WENO method for solving one-dimensional convection-dominated problem, and present the general parametrized flux limiting technique to maintain MPP and high order accuracy. A third order error analysis of general non-linear case is given to show that this limiting technique preserves high order accuracy without extra time-step restriction when the local Lax-Freidrich flux is chosen as part of the lower order flux. In Chapter 5, we shall discuss the FD RK WENO method with the general parametrized flux limiters for two-dimensional problems. We will demonstrate the desired performance of the proposed method in Chapter 6 by computing standard test problems, porous medium problems, Buckley-Leverett equations, and Navier-Stokes equations in vorticity stream-function formulation. Concluding remarks will be given in Chapter 7.

Chapter 2

ENO and WENO [26]

In this chapter, we give a brief introduction of ENO and WENO reconstruction in 1D case based on the lecture notes by Shu [26]. Some related research work could be found in [9, 8, 4, 10, 28, 29, 25]. The approximation problem will be discussed in both finite volume and finite difference methods.

Given the following discretization on the spatial domain $[a,b]$:

$$a = x_{\frac{1}{2}} < x_{\frac{3}{2}} < \cdots < x_{N-\frac{1}{2}} < x_{N+\frac{1}{2}} = b, \tag{2.1}$$

we define the grid, grid size and grid center by

$$I_j = [x_{j-\frac{1}{2}}, x_{j+\frac{1}{2}}], \quad x_j = \frac{1}{2}\left(x_{j-\frac{1}{2}} + x_{j+\frac{1}{2}}\right) \tag{2.2}$$

$$\Delta x_j = x_{j+\frac{1}{2}} - x_{j-\frac{1}{2}}, \quad j = 1, 2, \cdots, N. \tag{2.3}$$

We also denote the maximum of grid size by

$$\Delta x = \max_{1 \le j \le N} \Delta x_j. \tag{2.4}$$

2.1 Approximation problem in finite volume (FV) and finite difference (FD) schemes

2.1.1 Reconstruction from cell averages (FV scheme) [8]

Given the cell average of a function $v(x)$:

$$\bar{v}_i \equiv \frac{1}{\Delta x_i} \int_{x_{i-\frac{1}{2}}}^{x_{i+\frac{1}{2}}} v(\xi) d\xi, \quad i = 1, 2, \cdots, N, \tag{2.5}$$

we want to find a polynomial $p_i(x)$, of degree at most $k-1$, such that

$$v(x) = p_i(x) + \mathscr{O}(\Delta x^k), \quad x \in I_i, \quad i = 1, 2, \cdots, N \tag{2.6}$$

Correspondingly, the value of function $v(x)$ at the cell boundaries could be evaluated by

$$v^-_{i+\frac{1}{2}} = p_i(x_{i+\frac{1}{2}}), \quad v^+_{i-\frac{1}{2}} = p_i(x_{i-\frac{1}{2}}). \tag{2.7}$$

To make such a kth order accurate approximation to the function $v(x)$ at the boundaries of cell I_i, where $i = 1, 2, \cdots, N.$, we first choose a "stencil" $S(i)$:

$$\{I_{i-r}, \cdots, I_i, \cdots, I_{i+s}\} \tag{2.8}$$

which includes $r + s + 1 = k$ cells.

Suppose the primitive function of $v(x)$ is denoted by

$$V(x) \equiv \int_{-\infty}^{x} v(\xi) d\xi, \tag{2.9}$$

we could have $V'(x) = v(x)$ based on the fundamental theorem of calculus. Then there exits a unique polynomial $P(x)$, of degree at most k, which interpolates $V(x)$ over the points $x_{i-r-\frac{1}{2}}, \cdots, x_{i+s+\frac{1}{2}}$. Denote the derivative of $P(x)$ by $p(x) \equiv P'(x)$. Then we could have

$$\begin{aligned}
\frac{1}{\Delta x_i} \int_{x_{i-\frac{1}{2}}}^{x_{i+\frac{1}{2}}} p(\xi) d\xi &= \frac{1}{\Delta x_i} \left(P(x_{i+\frac{1}{2}}) - P(x_{i-\frac{1}{2}}) \right) \\
&= \frac{1}{\Delta x_i} (V(x_{i+\frac{1}{2}}) - V(x_{i-\frac{1}{2}})) \\
&= \frac{1}{\Delta x_i} \int_{x_{i-\frac{1}{2}}}^{x_{i+\frac{1}{2}}} v(\xi) d\xi \\
&= \bar{v}_i
\end{aligned} \tag{2.10}$$

and

$$V'(x) = P'(x) + \mathscr{O}(\Delta x^k). \tag{2.11}$$

Therefore, this $p(x)$ is exactly the polynomial we are looking for the approximation problem. Due to the form of polynomial, it's not hard to find that the mapping from cell averages to the point value at the cell boundaries is linear. Hence, there exist coefficients c_{rj} and $\tilde{c}_{rj}$, which could be obtained from the Lagrange form of interpolation polynomial, dependent on the left shift r of stencil $S(i)$, on the order of accuracy k, and on the cell sizes Δx_i in the stencil $S(i)$, but not on the function v, such that

$$v^-_{i+\frac{1}{2}} = \sum_{j=0}^{k-1} c_{rj} \bar{v}_{i-r+j}, \quad v^+_{i-\frac{1}{2}} = \sum_{j=0}^{k-1} \tilde{c}_{rj} \bar{v}_{i-r+j}, \quad r = 0, 1, \cdots, k-1. \tag{2.12}$$

We could also eliminate the superscripts $\pm$ since it's not hard to check that $\tilde{c}_{rj} = c_{r-1,j}$. In a summary, given the k cell averages of function $v(x)$:

$$\bar{v}_{i-r}, \cdots, \bar{v}_{i+s}, \tag{2.13}$$

there are constants c_{rj} such that the function $v(x)$ at the cell boundaries could be reconstructed by

$$v_{i+\frac{1}{2}} = \sum_{j=0}^{k-1} c_{rj} \bar{v}_{i-r+j}. \tag{2.14}$$

2.1.2 Reconstruction from point values (FD scheme)[28, 29]

Given the point values of a function $v(x)$:

$$v_i \equiv v(x_i), \tag{2.15}$$

we want to find a numerical flux

$$\hat{v}_{i+\frac{1}{2}} \equiv \hat{v}(v_{i-r}, \cdots, v_{i+s}), \quad i = 1, 2, \cdots, N \tag{2.16}$$

such that

$$\frac{1}{\Delta x_i}(\hat{v}_{i+\frac{1}{2}} - \hat{v}_{i-\frac{1}{2}}) = v'(x_i) + \mathscr{O}(\Delta x^k), \tag{2.17}$$

where $r+s+1 = k$, and the chosen stencil is $S(i) = \{I_{i-r}, \cdots, I_{i+s}\}$.

To solve this problem, we assume the uniform grid size, which is essential in FD scheme. If there is a function $h(x)$, such that

$$v(x) = \frac{1}{\Delta x} \int_{x-\frac{\Delta x}{2}}^{x+\frac{\Delta x}{2}} h(\xi) d\xi, \tag{2.18}$$

then it's not hard to see

$$v'(x_i) = \frac{1}{\Delta x}(h(x_{i+\frac{1}{2}}) - h(x_{i-\frac{1}{2}})). \tag{2.19}$$

Therefore,we could use

$$\hat{v}_{i+\frac{1}{2}} = h(x_{i+\frac{1}{2}}) + \mathscr{O}(\Delta x^k). \tag{2.20}$$

Specifically, we notice that v_i could be identified as the cell average of the unknown function $h(x)$, hence we could follow the same procedure discussed in FV scheme to reconstruct the value of function $h(x)$ at the cell boundaries using its cell averages. In a summary, given the k point values of function $v(x)$:

$$v_{i-r}, \cdots, v_{i+s}, \tag{2.21}$$

where $r+s+1=k$, there exist constants c_{rj} such that the required numerical flux $\hat{v}_{i+\frac{1}{2}}$ could be reconstructed by

$$\hat{v}_{i+\frac{1}{2}} = \sum_{j=0}^{k-1} c_{rj} v_{i-r+j}, \tag{2.22}$$

where c_{rj} could be found from Lagrange interpolation process.

2.1.3 Fixed stencil

By fixed stencil, we mean the left shift r of stencil $S(i)$ is always the same for all positions $i = 1, 2, \cdots, N$. For the globally smooth function, the fixed stencil is good enough to make the reconstruction. For example, to have a 3rd order accurate approximation to $v(x_{i+\frac{1}{2}})$, one could always choose the stencil $\{I_{i-1}, I_i, I_{i+1}\}$. However, when the function is piecewise

smooth, the reconstruction with fixed stencil may not be satisfactory. Specifically, the oscillation may show up near the discontinuity of the function, since the cell which involves the discontinuity may be included by the chosen fixed stencil.

2.2 ENO

To avoid containing the discontinuous cell in the stencil, if possible, a new idea called "adaptive stencil " was motivated. That is, the left shift r of the stencil $S(i)$ changes with the location i. To achieve this effect, Newton formulation of the interpolation polynomial was studied and the Newton divided difference of the function $V(x)$ in (2.9), as defined below, was identified as a measurement of the smoothness of the function of interest over the stencil [8]. The smaller divided difference implies a "smoother" function in that stencil. Specifically, the 0th divided difference of the function $V(x)$ is defined as:

$$V[x_{i-\frac{1}{2}}] \equiv V(x_{i-\frac{1}{2}}), \tag{2.23}$$

and the jth degree divided difference, for $j \geq 1$, is defined inductively by

$$V[x_{i-\frac{1}{2}}, \cdots, x_{i+j-\frac{1}{2}}] \equiv \frac{V[x_{i+\frac{1}{2}}, \cdots, x_{i+j-\frac{1}{2}}] - V[x_{i-\frac{1}{2}}, \cdots, x_{i+j-\frac{3}{2}}]}{x_{i+j-\frac{1}{2}} - x_{i-\frac{1}{2}}}. \tag{2.24}$$

Now, to determine the local stencil, we begin with one cell

$$S(i) = \{I_i\}, \tag{2.25}$$

and add one cell from the two neighbouring candidates I_{i-1} and I_{i+1}, by comparing the corresponding Newton divided difference of the function $V(x)$ and choosing the one with a less absolute value. Specifically,

· If $|V[x_{i-\frac{3}{2}}, x_{i-\frac{1}{2}}, x_{i+\frac{1}{2}}]| < |V[x_{i-\frac{1}{2}}, x_{i+\frac{1}{2}}, x_{i+\frac{3}{2}}]|$,
$S(i) = \{I_{i-1}, I_i\}$;

· Otherwise,
$S(i) = \{I_i, I_{i+1}\}$.

Then we continue this procedure by adding one cell into the stencil at each step until the required number of points are obtained in the stencil.

2.3 WENO

WENO [17, 11] is developed based upon ENO and, instead of using only one candidate stencil, it uses a convex linear combination of reconstruction results from all possible stencils so that the order of accurate could be improved.

Suppose there are k candidate stencils:

$$S_r(i) = \{I_{i-r}, \cdots, I_{i+k-r-1}\}, \quad r = 0, 1, \cdots, k-1. \tag{2.26}$$

Then correspondingly, we could have k different reconstructions as

$$v_{i+\frac{1}{2}}^{(r)} = \sum_{j=0}^{k-1} c_{rj} \bar{v}_{i-r+j}, \quad r = 0, 1, \cdots, k-1. \tag{2.27}$$

Here we take the reconstruction from cell averages as example, while the one from point values is exactly the same. By taking a convex combination of these k reconstruction

results, we have

$$v_{i+\frac{1}{2}} = \sum_{r=0}^{k-1} w_r v_{i+\frac{1}{2}}^{(r)}, \tag{2.28}$$

where w_r are constant weights that satisfy conditions of stability and consistency:

$$w_r \geq 0, \quad \sum_{r=0}^{k-1} w_r = 1. \tag{2.29}$$

To have a $(2k-1)$th order accurate approximation:

$$v_{i+\frac{1}{2}} = v(x_{i+\frac{1}{2}}) + \mathscr{O}(\Delta x^k), \quad i = 1, 2, \cdots, N, \tag{2.30}$$

the weights w_r are calculated by

$$w_r = \frac{\alpha_r}{\sum_{s=0}^{k-1} \alpha s}, \quad r = 0, \cdots, k-1 \tag{2.31}$$

with

$$\alpha_r = \frac{d_r}{(\varepsilon + \beta_r)^2}, \tag{2.32}$$

$$\beta_r = \sum_{l=1}^{k-1} \int_{x_{i-\frac{1}{2}}}^{x_{i+\frac{1}{2}}} \Delta x^{2l-1} \left(\frac{\partial^l p_r(x)}{\partial x^l} \right) dx, \tag{2.33}$$

where $\varepsilon > 0$ is introduced to avoid the denominator to be 0, $p_r(x)$ is the reconstruction polynomial on the stencil $S_r(i)$, β_r's [11] are the "smooth indicators" and d_r's are the linear weights when the function is smooth in all of the candidate stencils, which are all positive and satisfy

$$\sum_{r=0}^{k-1} d_r = 1. \tag{2.34}$$

Chapter 3

MPP high order FV WENO scheme for convection diffusion equations [35]

In [36], for the first time, a high order MPP method for multidimensional nonlinear scalar conservation laws was proposed within FV or discontinuous Galerkin schemes. Some suitable generalizations and developments could be found in [31, 37, 39, 40, 38]. The method was later generalized to convection diffusion equations by Zhang et al. in [35]. In this chapter, we review the main idea in [35] and describe this nonconventional MPP high order FV WENO scheme with both theoretical results and implementation details in one dimensional case. The two-dimensional extensions are straightforward, which we refer to [35] for details.

3.1 FV scheme with Euler forward time discretization solving conservation laws

Given the 1D scalar conservation laws (1.4), we consider a uniform mesh on domain $[a,b]$:

$$a = x_{\frac{1}{2}} < x_{\frac{3}{2}} < \cdots < x_{N-\frac{1}{2}} < x_{N+\frac{1}{2}} = b, \tag{3.1}$$

with

$$I_j = [x_{j-\frac{1}{2}}, x_{j+\frac{1}{2}}], \quad x_j = \frac{x_{j+\frac{1}{2}} + x_{j-\frac{1}{2}}}{2}, \quad \Delta x = \frac{b-a}{N}. \tag{3.2}$$

Integrate (1.4) over the cell I_j, we could obtain:

$$\frac{d\bar{u}(x_j,t)}{dt} = -\frac{1}{\Delta x}(f(u(x_{j+\frac{1}{2}},t)) - f(u(x_{j-\frac{1}{2}},t))), \tag{3.3}$$

where

$$\bar{u}(x_j,t) = \frac{1}{\Delta x}\int_{x_{j-\frac{1}{2}}}^{x_{j+\frac{1}{2}}} u(\xi,t)d\xi. \tag{3.4}$$

So a conservative finite volume scheme with Euler forward time discretization has the form:

$$\bar{u}_j^{n+1} = \bar{u}_j^n - \frac{\Delta t}{\Delta x}[\hat{f}(u^-_{j+\frac{1}{2}}, u^+_{j+\frac{1}{2}}) - \hat{f}(u^-_{j-\frac{1}{2}}, u^+_{j-\frac{1}{2}})], \tag{3.5}$$

where Δt is the uniform time step size, $\bar{u}_j^n$ is the approximation to $\bar{u}(x_j,t^n)$ in the cell I_j, and $u^-_{j+\frac{1}{2}}$, $u^+_{j+\frac{1}{2}}$ are the approximations to $u(x_{j+\frac{1}{2}},t^n)$ within the cells I_j and I_{j+1} respectively. The numerical flux $\hat{f}$ is a monotone flux, which satisfies [26]:

- $\hat{f}$ is a Lipschitz continuous in both arguments;
- $\hat{f}$ is nondecreasing in first argument and nonincreasing in second argument. Symbolically $\hat{f}(\uparrow,\downarrow)$;
- $\hat{f}$ is consistent with the physical flux f: $\hat{f}(u,u) = f(u)$.

A common choice of $\hat{f}$ is Lax-Friedrich flux. Suppose the polynomial $p_j(x)$ defined on I_j is used to approximate relevant cell averages and point values, that is, $\bar{u}_j^n$ is the cell average of $p_j(x)$ on I_j, $u^+_{j-\frac{1}{2}} = p_j(x_{j-\frac{1}{2}})$ and $u^-_{j+\frac{1}{2}} = p_j(x_{j+\frac{1}{2}})$. Then theorem 2.2 in [36] shows that the monotonicity of the right-hand side of (3.5) with respect to some point values of $p_j(x)$ is a sufficient condition for $\bar{u}_j^{n+1} \in [u_m, u_M]$, if $p_j(x) \in [u_m, u_M]\ \forall x \in I_j$. Based on the consideration of this crucial "monotonicity", a non-conventional high order FV scheme for convection diffusion equations was developed in [35].

3.2 FV scheme with Euler forward time discretization solving convection diffusion equations

To solve the convection diffusion equation, it looks natural to generalize the idea solving conservation laws directly. However, it seems extremely hard to do so. In the general conservative FV scheme solving convection diffusion equation, which is derived from integrating equation over I_j, a numerical flux is needed to approximate the spatial derivatives, not the function itself alone. This results in that the monotonicity, as stated in the end of last section, can only be achievable for first and second order approximation in this case. Therefore, to have arbitrary high order approximation, Zhang et al. [35] introduced the double cell average to remove the spatial derivatives by integrating the equation (1.1) over the cell I_j twice.

Define the double cell average of a function $u(x)$ over the cell I_j as

$$\bar{\bar{u}}_j = \frac{1}{\Delta x^2}\int_{x_{j-\frac{1}{2}}}^{x_{j+\frac{1}{2}}}\left(\int_{x-\frac{\Delta x}{2}}^{x+\frac{\Delta x}{2}} u(\xi)d\xi\right)dx, \tag{3.6}$$

then a twice-integrated version of (1.1) could be obtained as

$$\begin{aligned}\frac{d\bar{\bar{u}}_j(t)}{dt}&+\frac{1}{\Delta x^2}\left(\int_{x_j}^{x_{j+1}} f(u(x))dx-\int_{x_{j-1}}^{x_j} f(u(x))dx\right)\\ &=\frac{1}{\Delta x^2}\left(A(u(x_{j+1})-2A(u(x_j))+A(u(x_{j-1}))\right).\end{aligned} \tag{3.7}$$

Replace the integral by quadrature, then we have

$$\begin{aligned}\frac{d\bar{\bar{u}}_j(t)}{dt}&+\frac{1}{\Delta x}\sum_{\alpha=1}^{3} w_\alpha\left(f(u(x^\alpha_{j+\frac{1}{2}}))-f(u(x^\alpha_{j-\frac{1}{2}}))\right)\\ &=\frac{1}{\Delta x^2}\left(A(u(x_{j+1})-2A(u(x_j))+A(u(x_{j-1}))\right),\end{aligned} \tag{3.8}$$

where $x^\alpha_{j+\frac{1}{2}}$ are Gauss quadrature points on the interval $[x_j, x_{j+1}]$, defined by

$$x^\alpha_{j+\frac{1}{2}} = x_{j+\frac{1}{2}} + x_\alpha \Delta x, \quad \alpha = 1,2,3, \tag{3.9}$$

with x_α and w_α as Legendre Gauss quadrature points and weights on $[-\frac{1}{2},\frac{1}{2}]$:

$$x_\alpha = \{-\frac{\sqrt{15}}{10}, 0, \frac{\sqrt{15}}{10}\}, \quad w^\alpha = \{\frac{5}{18}, \frac{4}{9}, \frac{5}{18}\}. \tag{3.10}$$

Furthermore, to make a high order accurate approximation to $u(x)$, Zhang et al. in [35] introduced a fifth order WENO reconstruction method based on double cell averages by giving the table of linear weights for different kinds of quadrature points as well as deriving the smoothness indicators and nonlinear weights. For details, we refer to section 2 in [35].

Finally, a FV WENO scheme with Euler forward time discretization can be written as

$$\bar{\bar{u}}_j^{n+1} = \bar{\bar{u}}_j^n - \lambda \sum_{\alpha=1}^{3} w_\alpha \left(\hat{f}(u_{j+\frac{1}{2}}^{\alpha,-}, u_{j+\frac{1}{2}}^{\alpha,+}) - \hat{f}(u_{j-\frac{1}{2}}^{\alpha,-}, u_{j-\frac{1}{2}}^{\alpha,+}) \right) \tag{3.11}$$

$$+ \mu \left(A(u_{j+1}) - 2A(u_j) + A(u_{j-1}) \right), \tag{3.12}$$

where $\lambda = \frac{\Delta t}{\Delta x}$ and $\mu \frac{\Delta t}{\Delta x^2}$, $\bar{\bar{u}}_j^n$ is the approximation to the double cell average of $u(x,t)$ on the cell I_j at nth time step, and $u_{j-\frac{1}{2}}^{\alpha,+}$, $u_{j+\frac{1}{2}}^{\alpha,-}$, u_i are the fifth order WENO reconstructions of the point values $u(x_{j-\frac{1}{2}}^{\alpha})$, $u(x_{j+\frac{1}{2}}^{\alpha})$, $u(x_j)$, respectively, based on the stencil $S = \{I_{j-2}, \cdots, I_{j+2}\}$. The numerical flux $\hat{f}$ is chosen as the same as stated in section 3.1.

The scheme (3.11) could be further written as the sum of two parts:

$$\bar{\bar{u}}_j^{n+1} = \frac{1}{2} \sum_{\alpha=1}^{3} w_\alpha C_\alpha + \frac{1}{2} D, \tag{3.13}$$

where

$$C_\alpha = \bar{\bar{u}}_j^n - 2\lambda \left(\hat{f}(u_{j+\frac{1}{2}}^{\alpha,-}, u_{j+\frac{1}{2}}^{\alpha,+}) - \hat{f}(u_{j-\frac{1}{2}}^{\alpha,-}, u_{j-\frac{1}{2}}^{\alpha,+}) \right), \tag{3.14}$$

$$D = \bar{\bar{u}}_j^n + 2\mu (A(u_{j+1}) - 2A(u_j) + A(u_{j-1})). \tag{3.15}$$

Denote

$$H_\lambda(u_{j-1}^n, u_j^n, u_{j+1}^n) \equiv u_j^n - \lambda \left(\hat{f}(u_j^n, u_{j+1}^n) - \hat{f}(u_{j-1}^n, u_j^n) \right). \tag{3.16}$$

It's not hard to prove that the function $H_\lambda(a,b,c)$ is increasing in all three arguments and the consistency $H_\lambda(a,a,a) = a$. Then, assume there exist two polynomials of degree four $p_j^\alpha(x)$ and $p_j(x)$ satisfying

- $p_j^\alpha(x) = u(x) + \mathcal{O}(\Delta x^5)$, $\forall x \in [x_{j-1}, x_{j+1}]$

- $\frac{1}{\Delta x^2}\int_{x_{j-\frac{1}{2}}}^{x_{j+\frac{1}{2}}}\int_{x-\frac{\Delta x}{2}}^{x+\frac{\Delta x}{2}} p_j^{\alpha}(\xi)d\xi dx = \bar{\bar{u}}_j^n$,

- $p_j^{\alpha}(x_{j-\frac{1}{2}}^{\alpha}) = u_{j-\frac{1}{2}}^{\alpha,+}$ and $p_j^{\alpha}(x_{j+\frac{1}{2}}^{\alpha}) = u_{j+\frac{1}{2}}^{\alpha,-}$,

- $p_j(x) = u(x) + \mathscr{O}(\Delta x^5)$, $\forall x \in [x_{j-1}, x_{j+1}]$,

- $\frac{1}{\Delta x^2}\int_{x_{j-\frac{1}{2}}}^{x_{j+\frac{1}{2}}}\int_{x-\frac{\Delta x}{2}}^{x+\frac{\Delta x}{2}} p_j(\xi)d\xi dx = \bar{\bar{u}}_j^n$, and $p_j(x) = u_j$,

the existence of which can be verified by interpolation, with the help of Gauss quadrature and mean value theorem, (3.14) and (3.15) can be written as

$$C_\alpha = (1-2\hat{w}_1 w_\alpha)p_j^{\alpha}(x_j^{\alpha,*}) + H_{\frac{2\lambda}{\hat{w}_1 w_\alpha}}(u_{j-\frac{1}{2}}^{\alpha,+}, u_{j+\frac{1}{2}}^{\alpha,-}, u_{j+\frac{1}{2}}^{\alpha,+}) + H_{\frac{2\lambda}{\hat{w}_1 w_\alpha}}(u_{j-\frac{1}{2}}^{\alpha,-}, u_{j-\frac{1}{2}}^{\alpha,+}, u_{j+\frac{1}{2}}^{\alpha,-}), \tag{3.17}$$

$$D = (1-\bar{w}_3)p_j(x_j^*) + \bar{w}_3\left(u_j - \frac{4\mu}{\bar{w}_3}A(u_j)\right) + 2\mu(A(u_{j+1}) + A(u_{j-1})). \tag{3.18}$$

where $\hat{w}_1 = \frac{1}{12}$ and $\bar{w}_3 = \frac{19}{54}$, H is defined in (3.16), the existence of $x_j^{\alpha,*}$ and x_j^* can be established by the mean value theorem, and both C_α and D are monotonically increasing function under the appropriate CFL conditions.

We cite the main theoretical result in [35]:

Theorem 1 *The scheme* (3.11) *satisfies the maximum principle, namely,* $\bar{\bar{u}}_j^{n+1} \in [u_m, u_M]$ *if* $u_{j\mp\frac{1}{2}}^{\alpha,\pm}$, $u_{j\pm\frac{1}{2}}^{\alpha,\pm}$, $p_j^{\alpha}(x_j^{\alpha,*})$, u_{j-1}, u_j, u_{j+1}, $p_j(x_j^*) \in [u_m, u_M]$ *under the CFL conditions*

$$\lambda \max_u |f'(u)| \le \frac{1}{2}\hat{w}_1 \min_\alpha w_\alpha = \frac{5}{432}, \quad \mu \max_u A'(u) \le \frac{1}{4}\bar{w}_3 = \frac{19}{216}. \tag{3.19}$$

3.3 Maximum-principle satisfying scheme

3.3.1 A linear scaling limiter

To control the reconstruction values in the range $[u_m, u_M]$, a linear scaling limiter was introduced in [16]. In particular, considering the reconstruction polynomial $p_j(x)$ defined on $[x_{j-1}, x_{j+1}]$ in FV WENO scheme, we define the scaled polynomial by

$$\tilde{p}_j(x) = \theta(p_j(x) - \bar{\bar{u}}_j) + \bar{\bar{u}}_j, \quad \theta = \min\{|\frac{u_M - \bar{\bar{u}}_j}{M_j - \bar{\bar{u}}_j}|, |\frac{u_m - \bar{\bar{u}}_j}{m_j - \bar{\bar{u}}_j}|, 1\}, \tag{3.20}$$

where u_m and u_M are as defined in (1.2),

$$M_j = \max_{x \in [x_{j-1}, x_{j+1}]} p_j(x), \quad m_j = \min_{x \in [x_{j-1}, x_{j+1}]} p_j(x). \tag{3.21}$$

It's not hard to check that the cell average of $\tilde{p}_j(x)$ is still $\bar{\bar{u}}_j$ and $\tilde{p}_j(x)$ remains in the range $[u_m, u_M]$ $\forall x \in [x_{j-1}, x_{j+1}]$ without destroying the accuracy [35].

3.3.2 Algorithm

The algorithm of the fifth order MPP WENO scheme with Euler forward time discretization could be summarized as below:

- At nth time step, given $\bar{\bar{u}}_j^n$ with $j = i-2, \cdots, i+2$, use WENO reconstruction to obtain point values $u_{j-\frac{1}{2}}^{\alpha,+}$, $u_{j+\frac{1}{2}}^{\alpha,-}$ and u_j;
- Revise the point values by linear scaling limiter:

(a) For each j and α,

$$\tilde{u}^{\alpha,\mp}_{j\pm\frac{1}{2}} = \theta(u^{\alpha,\mp}_{j\pm\frac{1}{2}} - \bar{\bar{u}}^n_j) + \bar{\bar{u}}^n_j, \quad \theta = \min\{|\frac{u_M - \bar{\bar{u}}_j}{M_j - \bar{\bar{u}}_j}|, |\frac{u_m - \bar{\bar{u}}_j}{m_j - \bar{\bar{u}}_j}|, 1\}, \quad (3.22)$$

with

$$M_j = \max\{u^{\alpha,-}_{j+\frac{1}{2}}, u^{\alpha,+}_{j-\frac{1}{2}}, p^\alpha_j(x^{\alpha,*}_j)\}, m_j = \min\{u^{\alpha,-}_{j+\frac{1}{2}}, u^{\alpha,+}_{j-\frac{1}{2}}, p^\alpha_j(x^{\alpha,*}_j)\}, \quad (3.23)$$

where $p^\alpha_j(x^{\alpha,*}_j) = \left(\bar{\bar{u}}^n_j - \frac{1}{12}w_\alpha(u^{\alpha,-}_{j+\frac{1}{2}} + u^{\alpha,+}_{j-\frac{1}{2}})\right) / \left(1 - \frac{1}{6}w_\alpha\right)$;

(b) For each j,

$$\tilde{u}_j = \theta(u_j - \bar{\bar{u}}^n_j) + \bar{\bar{u}}^n_j, \quad \theta = \min\{|\frac{u_M - \bar{\bar{u}}_j}{M_j - \bar{\bar{u}}_j}|, |\frac{u_m - \bar{\bar{u}}_j}{m_j - \bar{\bar{u}}_j}|, 1\}, \quad (3.24)$$

with

$$M_j = \max\{u_j, p_j(x^*_j)\}, \quad m_j = \min\{u_j, p_j(x^*_j)\} \quad (3.25)$$

where $p_j(x^*) = (\bar{\bar{u}}^n_j - \bar{w}_3 u_j)/(1 - \bar{w}_3)$.

· Revise the scheme:

$$\bar{\bar{u}}^{n+1}_j = \bar{\bar{u}}^n_j - \lambda \sum_{\alpha=1}^{3} w_\alpha \left(\hat{f}(\tilde{u}^{\alpha,-}_{j+\frac{1}{2}}, \tilde{u}^{\alpha,+}_{j+\frac{1}{2}}) - \hat{f}(\tilde{u}^{\alpha,-}_{j-\frac{1}{2}}, \tilde{u}^{\alpha,+}_{j-\frac{1}{2}})\right) \quad (3.26)$$

$$+ \mu(A(\tilde{u}_{j+1}) - 2A(\tilde{u}_j) + A(\tilde{u}_{j-1})). \quad (3.27)$$

3.3.3 High order time discretization

To have a full discretized high order scheme, we could use SSP high order time discretization. Take the third order SSP RK method as an example:

$$u^{(1)} = u^(n) + \Delta t L(u^(n)), \tag{3.28}$$

$$u^{(2)} = \frac{3}{4}u^{(n)} + \frac{1}{4}u^{(1)} + \frac{1}{4}\Delta t L(u^{(1)}), \tag{3.29}$$

$$u^{n+1} = \frac{1}{3}u^{(n)} + \frac{2}{3}u^{(2)} + \frac{2}{3}\Delta t L(u^{(2)}), \tag{3.30}$$

where $L(u)$ is the spatial operator.

Since an SSP high order time disctretizaion is a convex combination of Euler forward, the full discretized scheme will still satisfy MPP and the limiter introduced above needs to be applied to each stage of RK method.

Chapter 4

High order FD RK WENO scheme for 1D convection-dominated problem with MPP flux limiters [1]

In this chapter, we give the high order numerical scheme to solve the problem (1.1). We first consider the standard high order FD WENO [11] method to approximate the convection part and a high order central difference for the diffusion part. Both of those two approximations are in conservative form. Then, we will give a full description of how the general parametrized MPP flux limiters can be applied to solve (1.1) while satisfying the maximum principle with designed order of accuracy.

[1] The material contained in this chapter has been submitted for publication.

4.1 One dimensional FD RK WENO method

We first give a brief introduction to the regular high order FD WENO scheme solving the problem (1.1). Without loss of generality, we assume periodic boundary condition. Consider the uniform mesh (3.1) and definitions (3.2). Let $u_j(t)$ denote the value of solution at center point x_j at time t. Then the conventional finite difference scheme evolves the point values of the solution to the equation (1.1) in a semi-discretized conservative form:

$$\frac{d}{dt}u_j(t) + \frac{1}{\Delta x}(\hat{H}_{j+\frac{1}{2}} - \hat{H}_{j-\frac{1}{2}}) = \frac{1}{\Delta x}(\hat{H}^D_{j+\frac{1}{2}} - \hat{H}^D_{j-\frac{1}{2}}), \tag{4.1}$$

where $\hat{H}_{j+\frac{1}{2}}$ and $\hat{H}^D_{j+\frac{1}{2}}$ are the numerical fluxes for the convection and diffusion terms respectively.

For the convection part, $\hat{H}_{j+\frac{1}{2}} = \hat{f}(u_{j-r}, \cdots, u_{j+s})$ is Lipschitz continuous in all the arguments and consistent with the physical flux f. The stencil $\{x_{j-r}, \cdots, x_{j+s}\}$ is chosen upwind biased. Specifically, when $f'(u) \geq 0$, one more point from the left will be taken for reconstruction; otherwise, one more point from the right will be taken. When the sign of $f'(u)$ changes over the domain, we apply the Lax-Friedrichs flux splitting to the scheme. To obtain a high order accuracy in conservative spatial approximation, we adopt the WENO reconstruction reviewed in Chapter 2, where a sliding function $h(x)$ is considered such that

$$\frac{1}{\Delta x}\int_{x-\frac{\Delta x}{2}}^{x+\frac{\Delta x}{2}} h(\xi)d\xi = f(u(x,t)). \tag{4.2}$$

Differentiate (4.2) with respect to x, we have

$$\frac{1}{\Delta x}(h(x+\frac{\Delta x}{2}) - h(x-\frac{\Delta x}{2})) = f(u)_x. \tag{4.3}$$

Then the numerical flux $\hat{H}_{j+\frac{1}{2}}$ can be understood as an approximation to $h(x_{j+\frac{1}{2}})$, which could be reconstructed from neighboring cell averages of $h(x)$, $\bar{h}_k = \frac{1}{\Delta x}\int_{I_k} h(\xi)d\xi = f(u(x_k,t))$, $k = j-r,\ldots,j+s$. By adaptively assigning nonlinear weights to neighboring candidate stencils and taking the convex combination of all reconstructions, the WENO method preserves high order accuracy of the linear scheme around smooth regions of the solution, while producing a sharp and essentially non-oscillatory resolution of discontinuities.

For the diffusion part, in order to obtain a conservative form with consistent order of accuracy, a high order central difference is generally needed. For example, to be consistent with the fifth order WENO (WENO5) scheme, we can choose sixth order central difference scheme

$$f''(x_j) = \frac{2f_{j+3} - 27f_{j+2} + 270f_{j+1} - 490f_j + 270f_{j-1} - 27f_{j-2} + 2f_{j-3}}{180\Delta x^2} + \mathscr{O}(\Delta x^6), \quad (4.4)$$

where f_j denotes the value of any smooth function $f(x)$ at x_j. And the numerical flux in (4.1) could be correspondingly written as

$$\hat{H}^D_{j+\frac{1}{2}} = \frac{2A(u_{j+3}) - 25A(u_{j+2}) + 245A(u_{j+1}) - 245A(u_j) + 25A(u_{j-1}) - 2A(u_{j-2})}{180\Delta x}, \quad (4.5)$$

where u_j denotes the value of solution at x_j.

To describe the main algorithm in a fully discretized formulation with high order accuracy, we use the third order total variation diminishing (TVD) RK time discretization [28] below

as an example

$$\begin{aligned} u^{(1)} &= u^n + \Delta t L(u^n), \\ u^{(2)} &= u^n + \Delta t(\frac{1}{4}L(u^n) + \frac{1}{4}L(u^{(1)})), \\ u^{n+1} &= u^n + \Delta t(\frac{1}{6}L(u^n) + \frac{2}{3}L(u^{(2)}) + \frac{1}{6}L(u^{(1)})), \end{aligned} \tag{4.6}$$

with $L(u^n) \doteq -\frac{1}{\Delta x}(\hat{H}^{(n)}_{j+\frac{1}{2}} - \hat{H}^{(n)}_{j-\frac{1}{2}}) + \frac{1}{\Delta x}(\hat{H}^{D(n)}_{j+\frac{1}{2}} - \hat{H}^{D(n)}_{j-\frac{1}{2}})$, and u^n is the value at nth time step. $\hat{H}^{(n)}_{j+\frac{1}{2}}$ and $\hat{H}^{D(n)}_{j+\frac{1}{2}}$ are the numerical fluxes from WENO reconstruction and central difference scheme based on u^n respectively. Similarly, let $\hat{H}^{(1)}_{j+\frac{1}{2}}$ and $\hat{H}^{D(1)}_{j+\frac{1}{2}}$ be the numerical fluxes reconstructed based on $u^{(1)}$, $\hat{H}^{(2)}_{j+\frac{1}{2}}$ and $\hat{H}^{D(2)}_{j+\frac{1}{2}}$ be the numerical fluxes reconstructed based on $u^{(2)}$. Then we could evolve the numerical solution from nth time step to $(n+1)$th time step in a compressed form

$$u^{n+1}_j = u^n_j - \lambda(\hat{H}^{rk}_{j+\frac{1}{2}} - \hat{H}^{rk}_{j-\frac{1}{2}}), \tag{4.7}$$

where

$$\hat{H}^{rk}_{j+\frac{1}{2}} = \frac{1}{6}(\hat{H}^{(n)}_{j+\frac{1}{2}} - \hat{H}^{D(n)}_{j+\frac{1}{2}}) + \frac{1}{6}(\hat{H}^{(1)}_{j+\frac{1}{2}} - \hat{H}^{D(1)}_{j+\frac{1}{2}}) + \frac{2}{3}(\hat{H}^{(2)}_{j+\frac{1}{2}} - \hat{H}^{D(2)}_{j+\frac{1}{2}}) \tag{4.8}$$

with $\lambda = \frac{\Delta t}{\Delta x}$.

Following the general parametrized flux limiting method proposed in [32] for pure convection problems, we apply the flux limiting method introduced by Xu [33] to modify the integrated flux $\hat{H}^{rk}_{j+\frac{1}{2}}$ to preserve maximum principle with designed overall high order of accuracy.

4.2 1D parametrized MPP flux limiters

The FD RK WENO scheme provides an approximation with high order of accuracy , however, it does not guarantee that the numerical solution satisfies the maximum principle when solving (1.1). In [33], a class of parametrized flux limiters are derived to provide a sufficient condition for conservative schemes satisfying the discrete maximum principle. Xiong et al. [32] further generalized this parametrized flux limiting method by applying the MPP flux limiter at the final stage of RK time discretization only, instead of at each intermediate stage. Below, in the same spirit of the work proposed in [32], we give a full description of applying the parametrized flux limiters to the formulation (4.7).

To preserve the MPP property,

$$u_m \leq u_j^{n+1} \leq u_M, \quad \forall j, n, \tag{4.9}$$

where u_m and u_M are defined as in (1.2), we replace the numerical flux $\hat{H}^{rk}_{j+\frac{1}{2}}$ in (4.7) by the modified one

$$\tilde{H}^{rk}_{j+\frac{1}{2}} = \theta_{j+\frac{1}{2}}(\hat{H}^{rk}_{j+\frac{1}{2}} - \hat{h}_{j+\frac{1}{2}}) + \hat{h}_{j+\frac{1}{2}}, \tag{4.10}$$

where $\hat{h}_{j+\frac{1}{2}}$ is the low order monotone flux that satisfies the MPP property. The limiting parameters $\theta_{j+\frac{1}{2}}$'s are numbers defined in the interval $[0,1]$ such that

$$u_m \leq u_j^n - \lambda(\tilde{H}^{rk}_{j+\frac{1}{2}} - \tilde{H}^{rk}_{j-\frac{1}{2}}) \leq u_M, \tag{4.11}$$

which are separated into the following two inequalities for discussion

$$\lambda\theta_{j-\frac{1}{2}}(\hat{H}^{rk}_{j-\frac{1}{2}}-\hat{h}_{j-\frac{1}{2}})-\lambda\theta_{j+\frac{1}{2}}(\hat{H}^{rk}_{j+\frac{1}{2}}-\hat{h}_{j+\frac{1}{2}})-\Gamma^{M}_{j} \leq 0, \tag{4.12}$$

$$\lambda\theta_{j-\frac{1}{2}}(\hat{H}^{rk}_{j-\frac{1}{2}}-\hat{h}_{j-\frac{1}{2}})-\lambda\theta_{j+\frac{1}{2}}(\hat{H}^{rk}_{j+\frac{1}{2}}-\hat{h}_{j+\frac{1}{2}})-\Gamma^{m}_{j} \geq 0 \tag{4.13}$$

for further discussion. By decoupling the above two inequalities, the parameter $\theta_{j+\frac{1}{2}}$ can be obtained such that the modified scheme overall is still locally conservative and consistent. We introduce the notation $\Gamma^{M}_{j},\Gamma^{m}_{j}$ as

$$\Gamma^{M}_{j}=u_{M}-u^{n}_{j}+\lambda(\hat{h}_{j+\frac{1}{2}}-\hat{h}_{j-\frac{1}{2}})\geq 0, \quad \Gamma^{m}_{j}=u_{m}-u^{n}_{j}+\lambda(\hat{h}_{j+\frac{1}{2}}-\hat{h}_{j-\frac{1}{2}})\leq 0.$$

Similar to what is described in [33], we denote

$$F_{j\pm\frac{1}{2}}=\hat{H}^{rk}_{j\pm\frac{1}{2}}-\hat{h}_{j\pm\frac{1}{2}}$$

and decouple the inequalities (4.12) (4.13) for the limiting parameters in the following:

1. In the maximum value case, we consider the jth node. We first look for a locally defined pair of numbers $(\Lambda^{M}_{-\frac{1}{2},I_j},\Lambda^{M}_{+\frac{1}{2},I_j})$ such that if

   $$\theta_{j-\frac{1}{2}}\in[0,\Lambda^{M}_{-\frac{1}{2},I_j}], \quad \theta_{j+\frac{1}{2}}\in[0,\Lambda^{M}_{+\frac{1}{2},I_j}],$$

   then the inequality (4.12) holds. The existence of such pair of numbers is obvious since one can always let $(\Lambda^{M}_{-\frac{1}{2},I_j},\Lambda^{M}_{+\frac{1}{2},I_j})=(0,0)$. However the pair $(0,0)$ is not the optimal pair we shall choose since it reduces the high order approximation to first order. Therefore, we apply the decoupling of (4.12) for the limiting parameters, introduced by Xu [33] in the following:

(a) If $F_{j-\frac{1}{2}} \leq 0$ and $F_{j+\frac{1}{2}} \geq 0$,

$$(\Lambda^M_{-\frac{1}{2},I_j}, \Lambda^M_{+\frac{1}{2},I_j}) = (1,1).$$

(b) If $F_{j-\frac{1}{2}} \leq 0$ and $F_{j+\frac{1}{2}} < 0$,

$$(\Lambda^M_{-\frac{1}{2},I_j}, \Lambda^M_{+\frac{1}{2},I_j}) = (1, \min(1, \frac{\Gamma^M_j}{-\lambda F_{j+\frac{1}{2}}})).$$

(c) If $F_{j-\frac{1}{2}} > 0$ and $F_{j+\frac{1}{2}} \geq 0$,

$$(\Lambda^M_{-\frac{1}{2},I_j}, \Lambda^M_{+\frac{1}{2},I_j}) = (\min(1, \frac{\Gamma^M_j}{\lambda F_{j-\frac{1}{2}}}), 1).$$

(d) If $F_{j-\frac{1}{2}} > 0$ and $F_{j+\frac{1}{2}} < 0$,

· if equation (4.12) is satisfied with $(\theta_{j-\frac{1}{2}}, \theta_{j+\frac{1}{2}}) = (1,1)$, then

$$(\Lambda^M_{-\frac{1}{2},I_j}, \Lambda^M_{+\frac{1}{2},I_j}) = (1,1).$$

· if equation (4.12) is not satisfied with $(\theta_{j-\frac{1}{2}}, \theta_{j+\frac{1}{2}}) = (1,1)$, then

$$(\Lambda^M_{-\frac{1}{2},I_j}, \Lambda^M_{+\frac{1}{2},I_j}) = (\frac{\Gamma^M_j}{\lambda F_{j-\frac{1}{2}} - \lambda F_{j+\frac{1}{2}}}, \frac{\Gamma^M_j}{\lambda F_{j-\frac{1}{2}} - \lambda F_{j+\frac{1}{2}}}).$$

2. Similarly, in the minimum value case, we consider the jth node. Again, we shall find a locally defined pair of numbers $(\Lambda^m_{-\frac{1}{2},I_j}, \Lambda^m_{+\frac{1}{2},I_j})$ such that if

$$\theta_{j-\frac{1}{2}} \in [0, \Lambda^m_{-\frac{1}{2},I_j}], \quad \theta_{j+\frac{1}{2}} \in [0, \Lambda^m_{+\frac{1}{2},I_j}],$$

then the inequality (4.13) holds. The pair can be obtained in the following separate cases:

(a) If $F_{j-\frac{1}{2}} \geq 0$ and $F_{j+\frac{1}{2}} \leq 0$,

$$(\Lambda^m_{-\frac{1}{2},I_j}, \Lambda^m_{+\frac{1}{2},I_j}) = (1,1).$$

(b) If $F_{j-\frac{1}{2}} \geq 0$ and $F_{j+\frac{1}{2}} > 0$,

$$(\Lambda^m_{-\frac{1}{2},I_j}, \Lambda^m_{+\frac{1}{2},I_j}) = (1, \min(1, \frac{\Gamma^m_j}{-\lambda F_{j+\frac{1}{2}}})).$$

(c) If $F_{j-\frac{1}{2}} < 0$ and $F_{j+\frac{1}{2}} \leq 0$,

$$(\Lambda^m_{-\frac{1}{2},I_j}, \Lambda^m_{+\frac{1}{2},I_j}) = (\min(1, \frac{\Gamma^m_j}{\lambda F_{j-\frac{1}{2}}}), 1).$$

(d) If $F_{j-\frac{1}{2}} < 0$ and $F_{j+\frac{1}{2}} > 0$,

· if equation (4.13) is satisfied with $(\theta_{j-\frac{1}{2}}, \theta_{j+\frac{1}{2}}) = (1,1)$, then

$$(\Lambda^m_{-\frac{1}{2},I_j}, \Lambda^m_{+\frac{1}{2},I_j}) = (1,1).$$

· if equation (4.13) is not satisfied with $(\theta_{j-\frac{1}{2}}, \theta_{j+\frac{1}{2}}) = (1,1)$, then

$$(\Lambda^m_{-\frac{1}{2},I_j}, \Lambda^m_{+\frac{1}{2},I_j}) = (\frac{\Gamma^m_j}{\lambda F_{j-\frac{1}{2}} - \lambda F_{j+\frac{1}{2}}}, \frac{\Gamma^m_j}{\lambda F_{j-\frac{1}{2}} - \lambda F_{j+\frac{1}{2}}}).$$

Since $\theta_{j+\frac{1}{2}}$, which affects both u^{n+1}_j and u^{n+1}_{j+1}, is chosen to satisfy both upper (4.12) and lower (4.13) bound of numerical solution, the locally defined limiting parameter $\theta_{j+\frac{1}{2}}$ is finally given as

$$\theta_{j+\frac{1}{2}} = \min(\Lambda^M_{+\frac{1}{2},I_j}, \Lambda^M_{-\frac{1}{2},I_{j+1}}, \Lambda^m_{+\frac{1}{2},I_j}, \Lambda^m_{-\frac{1}{2},I_{j+1}}), \tag{4.14}$$

which provides a sufficient condition for the scheme (4.7) with modified numerical fluxes (4.10) to satisfy the discrete maximum principle (1.3). When the proposed method is applied to solve

$$u_t + g(u)_x = \varepsilon u_{xx}, \tag{4.15}$$

we prove that the proposed method maintains the third order accuracy when a third order finite difference method is used. Since we are considering the convection dominated problems, in the following discussion, we focus on the case $\varepsilon \leq \Delta x$.

Theorem 2 *Consider solving convection-dominated diffusion equation* (4.15) *using a third order finite difference spatial discretization and a third order RK time discretization with the scheme written in equation* (4.7)*. Assume the global error,*

$$e_j^n = |u_j^n - u(x_j, t^n)| = \mathscr{O}(\Delta x^3 + \Delta t^3), \quad \forall n, j. \tag{4.16}$$

Consider applying the proposed MPP limiter to the numerical fluxes $\hat{H}^{rk}_{j+\frac{1}{2}}$ *in equation* (4.7)*, and taking* $\hat{h}_{j+\frac{1}{2}}$ *in equation* (4.10) *to be*

$$\hat{h}_{j+\frac{1}{2}} = \frac{1}{2}(g(u_j^n) + g(u_{j+1}^n)) + \frac{1}{2}\alpha_{j+\frac{1}{2}}(u_j^n - u_{j+1}^n) - \varepsilon\frac{(u_{j+1}^n - u_j^n)}{\Delta x}, \tag{4.17}$$

then

$$|\hat{H}^{rk}_{j+\frac{1}{2}} - \tilde{H}^{rk}_{j+\frac{1}{2}}| = \mathscr{O}(\Delta x^3 + \Delta t^3), \quad \forall j, \tag{4.18}$$

with CFL constraint $|\alpha_{j+\frac{1}{2}}\lambda + \frac{\varepsilon\lambda}{\Delta x}| \leq 1$*, where* $\lambda = \frac{\Delta t}{\Delta x}$ *and* $\alpha_{j+\frac{1}{2}} = \max\limits_{u\in[u_j, u_{j+1}]} |g'(u)|, \quad \forall j.$

Proof: We only consider maximum value part here, and the proof of minimum value part is similar. Our discussion is based upon four cases of limiters introduced in Section 4.2.

Without specifying, we use u_j as u_j^n in the proof below. According to the assumption (4.16), the difference between $u(x_j,t^n)$ and u_j^n is of third order, hence in the following proof we use $u(x_j,t^n)$ and u_j^n interchangeably when such high order difference is allowed.

Case (a) There is no limiter introduced in this case, therefore (4.18) holds.

Case (d) In this case, $F_{j-\frac{1}{2}} > 0$ and $F_{j+\frac{1}{2}} < 0$. It is sufficient to show that

$$\frac{\Gamma_j^M - (\lambda F_{j-\frac{1}{2}} - \lambda F_{j+\frac{1}{2}})}{\lambda F_{j-\frac{1}{2}} - \lambda F_{j+\frac{1}{2}}} F_{j+\frac{1}{2}} = \mathscr{O}(\Delta x^3 + \Delta t^3) \tag{4.19}$$

when $\Gamma_j^M < \lambda F_{j-\frac{1}{2}} - \lambda F_{j+\frac{1}{2}}$. Since $F_{j-\frac{1}{2}} > 0$ and $F_{j+\frac{1}{2}} < 0$, we have $0 < \frac{-F_{j+\frac{1}{2}}}{\lambda F_{j-\frac{1}{2}} - \lambda F_{j+\frac{1}{2}}} \leq \frac{1}{\lambda}$. Recalling

$$\Gamma_j^M - (\lambda F_{j-\frac{1}{2}} - \lambda F_{j+\frac{1}{2}}) = u_M - \{u_j - \lambda(\hat{H}^{rk}_{j+\frac{1}{2}} - \hat{H}^{rk}_{j-\frac{1}{2}})\} < 0, \tag{4.20}$$

it suffices to show

$$|u_M - \{u_j - \lambda(\hat{H}^{rk}_{j+\frac{1}{2}} - \hat{H}^{rk}_{j-\frac{1}{2}})\}| = \mathscr{O}(\Delta x^3 + \Delta t^3), \tag{4.21}$$

which can be verified by using assumption (4.16) since we have $u(x_j,t^{n+1}) \leq u_M \leq u_j^{n+1}$ and $u_j^{n+1} = u_j - \lambda(\hat{H}^{rk}_{j+\frac{1}{2}} - \hat{H}^{rk}_{j-\frac{1}{2}})$.

Case (b) In this case, $F_{j-\frac{1}{2}} \leq 0$ and $F_{j+\frac{1}{2}} < 0$. We only need to consider the case when

$$\Lambda_{+\frac{1}{2},I_j} = \frac{\Gamma_j^M}{-\lambda F_{j+\frac{1}{2}}} < 1 \tag{4.22}$$

with

$$\tilde{H}^{rk}_{j+\frac{1}{2}} - \hat{H}^{rk}_{j+\frac{1}{2}} = \frac{\Gamma_j^M + \lambda F_{j+\frac{1}{2}}}{-\lambda} = \frac{u_M - \{u_j - \lambda(\hat{H}^{rk}_{j+\frac{1}{2}} - \hat{h}_{j-\frac{1}{2}})\}}{-\lambda}. \tag{4.23}$$

Therefore, it's sufficient to prove

$$|u_M - \{u_j - \lambda(\hat{H}^{rk}_{j+\frac{1}{2}} - \hat{h}_{j-\frac{1}{2}})\}| = \mathscr{O}(\Delta x^3 + \Delta t^3). \tag{4.24}$$

To follow the discussion in [32] for pure convection problem, we let $f(u) = g(u) - \varepsilon u_x$. For high order RK flux, we have

$$\hat{H}^{rk}_{j+\frac{1}{2}} = \frac{1}{\Delta t}\int_{t^n}^{t^{n+1}} h(x_{j+\frac{1}{2}}, t)dt + \mathscr{O}(\Delta t^3) \tag{4.25}$$

$$= \frac{1}{6}h(x_{j+\frac{1}{2}}, t^n + \Delta t) + \frac{2}{3}h(x_{j+\frac{1}{2}}, t^n + \frac{\Delta t}{2}) + \frac{1}{6}h(x_{j+\frac{1}{2}}, t^n) + \mathscr{O}(\Delta t^3), \tag{4.26}$$

where the 3-point Gauss Lobatto quadrature is used to obtain (4.26), and the sliding average function h can be given as [28]

$$h(x_{j+\frac{1}{2}}, t) = f(u(x_{j+\frac{1}{2}}, t)) + \sum_{k=1}^{s} a_{2k}\Delta x^{2k}\left(\frac{\partial^{2k}}{\partial x^{2k}} f(u(x,t))\right)_{x=x_{j+\frac{1}{2}}} + \mathscr{O}(\Delta x^{2s+2}) \tag{4.27}$$

with properly defined $\{a_{2k}\}$ to ensure $(h(x_{j+\frac{1}{2}}, t) - h(x_{j-\frac{1}{2}}, t))/\Delta x = f_x(u(x_j, t)) + \mathscr{O}(\Delta x^{2s+1})$ for arbitrary s. For a third order approximation ($s = 1$), we take the first two terms in (4.27) to get

$$h(x_{j+\frac{1}{2}}, t) = f(u(x_{j+\frac{1}{2}}, t)) - \frac{\Delta x^2}{24}\left(\frac{\partial^2}{\partial x^2} f(u(x,t))\right)_{x=x_{j+\frac{1}{2}}} + \mathscr{O}(\Delta x^4). \tag{4.28}$$

By approximating the second derivative of f with central difference, we can rewrite function h as

$$h(x_{j+\frac{1}{2}}, t) = \frac{13}{12} f(u(x_{j+\frac{1}{2}}, t)) - \frac{1}{24}\left(f(u(x_{j+\frac{3}{2}}, t)) + f(u(x_{j-\frac{1}{2}}, t))\right) + \mathscr{O}(\Delta x^4). \tag{4.29}$$

Therefore,

$$
\begin{aligned}
&\frac{1}{\Delta t}\int_{t^n}^{t^{n+1}} h(x_{j+\frac{1}{2}},t)dt \\
=&\frac{1}{6}\left(\frac{13}{12}f(u(x_{j+\frac{1}{2}},t^n+\Delta t))-\frac{1}{24}(f(u(x_{j+\frac{3}{2}},t^n+\Delta t))+f(u(x_{j-\frac{1}{2}},t^n+\Delta t)))\right) \\
&+\frac{2}{3}\left(\frac{13}{12}f(u(x_{j+\frac{1}{2}},t^n+\frac{\Delta t}{2}))-\frac{1}{24}(f(u(x_{j+\frac{3}{2}},t^n+\frac{\Delta t}{2}))+f(u(x_{j-\frac{1}{2}},t^n+\frac{\Delta t}{2})))\right) \\
&+\frac{1}{6}\left(\frac{13}{12}f(u(x_{j+\frac{1}{2}},t^n))-\frac{1}{24}(f(u(x_{j+\frac{3}{2}},t^n))+f(u(x_{j-\frac{1}{2}},t^n)))\right)+\mathscr{O}(\Delta t^3+\Delta x^4) \\
=&\left(\frac{13}{72}f(u(\cdot,t^n+\Delta t))+\frac{13}{18}f(u(\cdot,t^n+\frac{\Delta t}{2}))+\frac{13}{72}f(u(\cdot,t^n))\right)\Big|_{x_{j+\frac{1}{2}}} \\
&-\left(\frac{1}{144}f(u(\cdot,t^n+\Delta t))+\frac{1}{36}f(u(\cdot,t^n+\frac{\Delta t}{2}))+\frac{1}{144}f(u(\cdot,t^n))\right)\Big|_{x_{j+\frac{3}{2}}} \\
&-\left(\frac{1}{144}f(u(\cdot,t^n+\Delta t))+\frac{1}{36}f(u(\cdot,t^n+\frac{\Delta t}{2}))+\frac{1}{144}f(u(\cdot,t^n))\right)\Big|_{x_{j-\frac{1}{2}}} \\
&+\mathscr{O}(\Delta t^3+\Delta x^4). \qquad (4.30)
\end{aligned}
$$

Since the f values involved at $t^n+\Delta t$ and $t^n+\frac{\Delta t}{2}$ are not directly available, we apply Taylor expansion to $f(u)$ in temporal direction around t^n to express (4.30) with relevant values at t^n. In order to implement the Taylor expansion, we find that

$$
\begin{aligned}
f(u)_t &= g'(u)u_t-\varepsilon u_{xt} \\
&= g'(u)(\varepsilon u_{xx}-g'(u)u_x)-\varepsilon(\varepsilon u_{xx}-g'(u)u_x)_x \qquad (4.31)
\end{aligned}
$$

and

$$\begin{aligned} f(u)_{tt} =&(g'(u))^2(3g''(u)u_x^2+g'(u)u_{xx}) \\ &+(-2(g''(u))^2u_x^3-12g'(u)g''(u)u_xu_{xx}-3g'(u)(g^{(3)}(u)u_x^3+g'(u)\frac{\partial^5 u}{\partial x^5}))\varepsilon \\ &+(g^{(4)}(u)u_x^4+7g^{(3)}(u)u_x^2u_{xx}+g''(u)(3u_x^2+2u_{xx}^2+6u_x\frac{\partial^3 u}{\partial x^3})+3g'(u)\frac{\partial^4 u}{\partial x^4})\varepsilon^2 \\ &-\frac{\partial^5 u}{\partial x^5}\varepsilon^3 \end{aligned} \tag{4.32}$$

by utilizing $f(u)=g(u)-\varepsilon u_x$ and the PDE $u_t=\varepsilon u_{xx}-g'(u)u_x$ repeatedly. Take $f(u(\cdot,t^n+\Delta t))$ for example, it can be written as

$$f(u(\cdot,t^n+\Delta t))=f(u(\cdot,t^n))+f(u)_t\Delta t+\frac{1}{2}f(u)_{tt}\Delta t^2+\mathscr{O}(\Delta t^3), \tag{4.33}$$

which can then be rewritten by replacing $f(u)_t$, $f(u)_{tt}$ with (4.31), (4.32). Therefore, (4.30) could be written into a form evaluated at t^n and $x_{j+\frac{k}{2}}$, where $k=\pm 1,3$. Central difference approximation of all the spatial derivatives turns out to be enough since the analysis is for third order schemes. Here we skip those forms to save some space.

In the following proof, we will use regular derivatives instead of partial derivatives for u since t is fixed at t^n. We first prove the case that the maximum or local maximum is reached inside the cell I_j, with $u_M=u(x_M)$, $u'_M=0$ and $u''_M\leq 0$. We perform Taylor expansions on u around x_M and on g around u_M. After simplification with the help of Mathematica and the convection dominating assumption $\varepsilon\leq\Delta x$, we have

$$\begin{aligned} &u_j-\lambda(\hat{H}^{rk}_{j+\frac{1}{2}}-\hat{h}_{j-\frac{1}{2}}) \\ =&u_M+\frac{u''_M}{12}(\Delta x)^2p(z,\lambda_0)+\mathscr{O}(\Delta x^3+\Delta t^3) \end{aligned} \tag{4.34}$$

with

$$\begin{aligned} p(z,\lambda_0) =& 6z^2 + 6z(\lambda_0^2 - 2\lambda_0 - \alpha_{j-\frac{1}{2}}\lambda) \\ &+ (-2\lambda_0^3 + 3\lambda_0^2 + 2\lambda_0 + 3\alpha_{j-\frac{1}{2}}\lambda + 12\frac{\varepsilon\lambda}{\Delta x} - 12\frac{\varepsilon\lambda}{\Delta x}\lambda_0), \end{aligned} \tag{4.35}$$

where $z = (x_j - x_M)/\Delta x$, $\lambda = \frac{\Delta t}{\Delta x}$, $\lambda_0 = g'(u_M)\lambda$ and $\alpha_{j-\frac{1}{2}} = \max\limits_{u\in[u_{j-1},u_j]} |g'(u)|$.

The minimum value for function p with respect to z is

$$\begin{aligned} p_{\min} &= p(z,\lambda_0)\Big|_{z=-\frac{1}{2}(-2\lambda_0-\gamma+\lambda_0^2)} \\ &= 2\lambda_0 + 3\gamma + 12c - 3\lambda_0^2 - 6\lambda_0\gamma - \frac{3\gamma^2}{2} - 12\lambda_0 c + 4\lambda_0^3 + 3\lambda_0^2\gamma - \frac{3\lambda_0^4}{2}, \end{aligned} \tag{4.36}$$

where $\gamma = \alpha_{j-\frac{1}{2}}\lambda$ and $c = \frac{\varepsilon\lambda}{\Delta x}$. It is easy to check that $|\lambda_0| - \gamma = \mathscr{O}(\Delta x)$ and $\lambda_0^2 - \gamma^2 = \mathscr{O}(\Delta x)$, therefore by replacing λ_0^2 by γ^2, we can write (4.36) as

$$\begin{aligned} p_{\min} &= p(z,\lambda_0)\Big|_{z=-\frac{1}{2}(-2\lambda_0-\gamma+\lambda_0^2)} \\ &= p_1(\lambda_0) + 12c(1-\lambda_0) + \mathscr{O}(\Delta x) \end{aligned} \tag{4.37}$$

with

$$p_1(\lambda_0) = 2(2\gamma-1)(\gamma-1)\lambda_0 + 3\gamma - \frac{9}{2}\gamma^2 + 3\gamma^3 - \frac{3}{2}\gamma^4. \tag{4.38}$$

Since it is straightforward to check that

$$p_1(-\gamma) = \frac{1}{2}\gamma(1-\gamma)(1+\gamma)(2+3\gamma) \geq 0, \tag{4.39}$$

$$p_1(\gamma) = \frac{1}{2}\gamma(1-\gamma)(2-\gamma)(5-3\gamma) \geq 0, \tag{4.40}$$

we have $p_1(\lambda_0) \geq 0$ for all $\lambda_0 \in [-\gamma,\gamma]$, which implies $p_1(\lambda_0) \geq \mathscr{O}(\Delta x)$ since $|\lambda_0| - \gamma =$

$\mathscr{O}(\Delta x)$. Combined with the fact that $12c(1-\lambda_0) \geq 0$, $p(z,\lambda_0) \geq p_{\min} \geq \mathscr{O}(\Delta x)$ holds. We thus have (4.24) since $u''_M \leq 0$.

Now if $u(x)$ reaches its maximum or local maximum at $x_{j-\frac{1}{2}}$, that is, $x_M = x_{j-\frac{1}{2}}$, then we have $u'(x_M) = u'_{j-\frac{1}{2}} \leq 0$. Following the previous calculation, we have

$$\begin{aligned} & u_j - \lambda(\hat{H}^{rk}_{j+\frac{1}{2}} - \hat{h}_{j-\frac{1}{2}}) \\ =& u(x_M) + u'(x_M)\Delta x s_1 + (u'(x_M))^2 \Delta x^2 s_2 + u''(x_M)\frac{\Delta x^2}{2} s_3 + \mathscr{O}(\Delta x^3 + \Delta t^3), \end{aligned} \tag{4.41}$$

where

$$s_1 = \frac{1}{2}(1 - 2\lambda_0 + \lambda_0^2) - \frac{1}{2}\gamma, \tag{4.42}$$

$$s_2 = -g''(u(x_M))\frac{\lambda}{6}(2 + 3\lambda_0^2 + 3c), \tag{4.43}$$

$$s_3 = \frac{1}{6}(\frac{3}{2} - 4\lambda_0 + 6\lambda_0^2 - 2\lambda_0^3) + 2c(1-\lambda_0) \tag{4.44}$$

with the same notation λ_0, γ and c. Again, considering $\lambda_0^2 - \gamma^2 = \mathscr{O}(\Delta x)$, we replace λ_0^2 by $\gamma^2 + c_1 \Delta x$ in (4.42), where c_1 is a constant, and rewrite (4.41) as

$$\begin{aligned} & u_j - \lambda(\hat{H}^{rk}_{j+\frac{1}{2}} - \hat{h}_{j-\frac{1}{2}}) \\ =& u(x_M - \sqrt{s_3}\Delta x) + (\sqrt{s_3} + \tilde{s}_1)\Delta x u'(x_M) + \Delta x^2 u'(x_M) s_4 + \mathscr{O}(\Delta t^3 + \Delta x^3) \end{aligned} \tag{4.45}$$

with

$$\tilde{s}_1 = \frac{1}{2}(1 - 2\lambda_0 + \gamma^2) - \frac{1}{2}\gamma \tag{4.46}$$

$$s_4 = u'(x_M)s_2 + c_1. \tag{4.47}$$

It's not hard to check that $s_3 \geq 0$ and $\sqrt{s_3} + \tilde{s}_1 \geq 0$ for $|\lambda_0| \leq \gamma \leq 1$. When $\lambda_0 \notin [-\gamma, \gamma]$, the proof is similar thanks to $|\lambda_0| - \gamma = \mathscr{O}(\Delta x)$. Therefore, to prove (4.24), it is sufficient to

show $u(x_M - \sqrt{s_3}\Delta x) + \Delta x^2 u'(x_M)s_4 \leq u_M$ or $u'(x_M) = \mathscr{O}(\Delta x)$. If $[x_M - \sqrt{s_3}\Delta x - \Delta x, x_M - \sqrt{s_3}\Delta x]$ is not a monotone region, there is a point $x^{(1)}$ in this region such that $u'(x^{(1)}) = 0$. If $[x_M - \sqrt{s_3}\Delta x - \Delta x, x_M - \sqrt{s_3}\Delta x]$ is a monotone increasing region, since $u'(x_M) < 0$, there is a point $x^{(2)}$ in this region such that $u'(x^{(2)}) = 0$. And for these two cases, $u'(x_M) = \mathscr{O}(\Delta x)$. Now, if $[x_M - \sqrt{s_3}\Delta x - \Delta x, x_M - \sqrt{s_3}\Delta x]$ is a monotonely decreasing region, we assume

$$u(x_M - \sqrt{s_3}\Delta x) + c_2\Delta x^2 > u_M, \tag{4.48}$$

where $c_2 = |u'(x_M)s_4|$. Since, according to mean value theorem, there is a point $x^{(3)}$ such that

$$u(x_M - \sqrt{s_3}\Delta x) = u(x_M - \sqrt{s_3}\Delta x - \Delta x) + u'(x^{(3)})\Delta x, \tag{4.49}$$

where $u'(x^{(3)}) < 0$. Then we have

$$u'(x^{(3)})\Delta x + c_2\Delta x^2 > 0, \tag{4.50}$$

which implies $|u'(x^{(3)})| < c_2\Delta x$, and hence, $u'(x_M) = \mathscr{O}(\Delta x)$.

When $x_M = x_{j+\frac{1}{2}}$, a similar proof could be presented. Therefore, combined with the discussion above, (4.24) is proved.

□

The choice of the low order monotone flux does not change the algorithm and implementation, however it will affect the accuracy of the scheme. As pointed out in [32], when global Lax-Friedrichs flux is used, a constraint of $CFL \leq 0.886$ is required to ensure high order accuracy and maximum principle.

Chapter 5

High order FD RK WENO scheme for 2D convection-dominated problem with MPP flux limiters [1]

The MPP flux limiters for two-dimensional scalar hyperbolic conservation laws are designed by Xu et al. in [15]. In this chapter, we're focusing on the generalization of the parametrized MPP flux limiters to the computation of the two-dimensional convection diffusion equations. Again, we will consider the regular FD RK WENO method for the two-dimensional problem first, and then apply the MPP flux limiters.

[1] The material contained in this chapter has been submitted for publication.

5.1 Two-dimensional FD RK WENO method

Consider the two-dimensional convection-diffusion equation

$$\begin{aligned} u_t + f(u)_x + g(u)_y &= A(u)_{xx} + B(u)_{yy}, \\ u(x,y,0) &= u_0(x,y), \quad (x,y) \in [a,b] \times [c,d], \end{aligned} \tag{5.1}$$

where $A'(u) \geq 0$ and $B'(u) \geq 0$. Assuming that we have uniform rectangular mesh

$$a = x_{\frac{1}{2}} < x_{\frac{3}{2}} < \cdots < x_{N-\frac{1}{2}} < x_{N+\frac{1}{2}} = b, \quad c = y_{\frac{1}{2}} < y_{\frac{3}{2}} < \cdots < y_{N-\frac{1}{2}} < y_{N+\frac{1}{2}} = d, \tag{5.2}$$

with grids, grid centers and grid size defined by

$$\Delta x = x_{i+\frac{1}{2}} - x_{i-\frac{1}{2}}, \quad x_i = \frac{1}{2}(x_{i+\frac{1}{2}} + x_{i-\frac{1}{2}}), \quad \Delta y = y_{j+\frac{1}{2}} - y_{j-\frac{1}{2}}, \quad y_j = \frac{1}{2}(y_{j+\frac{1}{2}} + y_{j-\frac{1}{2}}).$$

Then, we write the general conservative spatial approximation in the form

$$\begin{aligned} &\frac{u_{i,j}(t)}{dt} + \frac{1}{\Delta x}(\hat{H}_{i+\frac{1}{2},j} - \hat{H}_{i-\frac{1}{2},j}) + \frac{1}{\Delta y}(\hat{G}_{i,j+\frac{1}{2}} - \hat{G}_{i,j-\frac{1}{2}}) \\ &\quad = \frac{1}{\Delta x}(\hat{H}^D_{i+\frac{1}{2},j} - \hat{H}^D_{i-\frac{1}{2},j}) + \frac{1}{\Delta y}(\hat{G}^D_{i,j+\frac{1}{2}} - \hat{G}^D_{i,j-\frac{1}{2}}), \end{aligned} \tag{5.3}$$

where $u_{i,j}(t)$ is the numerical approximation to the point value $u(x_i, y_j, t)$. The construction of the high order spatial approximation is straightforward from the one dimensional scheme. For convection part, the numerical fluxes $\hat{H}_{i+\frac{1}{2},j}$, $\hat{G}_{i,j+\frac{1}{2}}$ are obtained from the one dimensional WENO reconstruction along x direction and y direction respectively. For

diffusion part, the numerical fluxes $\hat{H}^D_{i+\frac{1}{2},j}$ and $\hat{G}^D_{i,j+\frac{1}{2}}$ can be obtained from the high order central difference approximation in each of the direction.

By applying RK time discretization, similar to the one-dimensional scheme, the compressed high order finite difference RK WENO scheme could be finally written as

$$u^{n+1}_{i,j} = u^n_{i,j} - \lambda_x(\hat{H}^{rk}_{i+\frac{1}{2},j} - \hat{H}^{rk}_{i-\frac{1}{2},j}) - \lambda_y(\hat{G}^{rk}_{i,j+\frac{1}{2}} - \hat{G}^{rk}_{i,j-\frac{1}{2}}), \tag{5.4}$$

where $\lambda_x = \frac{\Delta t}{\Delta x}$ and $\lambda_y = \frac{\Delta t}{\Delta y}$. $\hat{H}^{rk}$ and $\hat{G}^{rk}$ can be understood as the average integral of the numerical fluxes in the temporal direction.

5.2 2D MPP parametrized flux limiters

Based on the regular FD RK WENO method described in the previous section, in this section we will apply the parametrized MPP flux limiters to the scheme (5.4). Let $u_m = \min_{x,y} u_0(x,y)$ and $u_M = \max_{x,y} u_0(x,y)$. In order to ensure the maximum principle, we are looking for the type of limiters

$$\begin{aligned} \tilde{H}^{rk}_{i+\frac{1}{2},j} &= \theta_{i+\frac{1}{2},j}(\hat{H}^{rk}_{i+\frac{1}{2},j} - \hat{h}_{i+\frac{1}{2},j}) + \hat{h}_{i+\frac{1}{2},j}, \\ \tilde{G}^{rk}_{i,j+\frac{1}{2}} &= \theta_{i,j+\frac{1}{2}}(\hat{G}^{rk}_{i,j+\frac{1}{2}} - \hat{g}_{i,j+\frac{1}{2}}) + \hat{g}_{i,j+\frac{1}{2}}, \end{aligned} \tag{5.5}$$

such that

$$u_m \le u^n_{i,j} - \lambda_x(\tilde{H}^{rk}_{i+\frac{1}{2},j} - \tilde{H}^{rk}_{i-\frac{1}{2},j}) - \lambda_y(\tilde{G}^{rk}_{i,j+\frac{1}{2}} - \tilde{G}^{rk}_{i,j-\frac{1}{2}}) \le u_M. \tag{5.6}$$

Here $\hat{h}_{i+\frac{1}{2},j}$,$\hat{g}_{i,j+\frac{1}{2}}$ are chosen as any low order monotone flux satisfying MPP property,

$$u_m \leq u_{i,j}^n - \lambda_x(\hat{h}_{i+\frac{1}{2},j} - \hat{h}_{i-\frac{1}{2},j}) - \lambda_y(\hat{g}_{i,j+\frac{1}{2}} - \hat{g}_{i,j-\frac{1}{2}}) \leq u_M. \tag{5.7}$$

The inequalities (5.6) with (5.5) form coupled constraint of the limiting parameters $\theta_{i+\frac{1}{2},j}$, $\theta_{i,j+\frac{1}{2}}$. Again, for the purpose of designing a locally conservative and consistent high order scheme, explicit values shall be sought by decoupling (5.6) with (5.5). Following the decoupling process described in [15], for each pair of node (i,j), the MPP limiters could be parametrized in the sense that we can find a group of numbers $\Lambda_{L,i,j}$, $\Lambda_{R,i,j}$, $\Lambda_{D,i,j}$, $\Lambda_{U,i,j}$ such that (5.6) holds for any group of numbers

$$(\theta_{i-\frac{1}{2},j}, \theta_{i+\frac{1}{2},j}, \theta_{i,j-\frac{1}{2}}, \theta_{i,j+\frac{1}{2}}) \in [0,\Lambda_{L,i,j}] \times [0,\Lambda_{R,i,j}] \times [0,\Lambda_{D,i,j}] \times [0,\Lambda_{U,i,j}]. \tag{5.8}$$

For the brevity of discussion, we denote

$$\begin{cases} F_{i-\frac{1}{2},j} = \lambda_x(\hat{H}^{rk}_{i-\frac{1}{2},j} - \hat{h}_{i-\frac{1}{2},j}), \\ F_{i+\frac{1}{2},j} = -\lambda_x(\hat{H}^{rk}_{i+\frac{1}{2},j} - \hat{h}_{i+\frac{1}{2},j}), \\ F_{i,j-\frac{1}{2}} = \lambda_y(\hat{G}^{rk}_{i,j-\frac{1}{2}} - \hat{g}_{i,j-\frac{1}{2}}), \\ F_{i,j+\frac{1}{2}} = -\lambda_y(\hat{G}^{rk}_{i,j+\frac{1}{2}} - \hat{g}_{i,j+\frac{1}{2}}). \end{cases} \tag{5.9}$$

For the maximum part, let

$$\Gamma^M_{i,j} = u_M - (u_{i,j} - \lambda_x(\hat{h}_{i+\frac{1}{2},j} - \hat{h}_{i-\frac{1}{2},j}) - \lambda_y(\hat{g}_{i,j+\frac{1}{2}} - \hat{g}_{i,j-\frac{1}{2}})) \geq 0, \tag{5.10}$$

when the monotone numerical flux is used under a suitable CFL constraint. The coupled inequality (5.6) with (5.5) can now be rewritten as

$$\theta_{i+\frac{1}{2},j}F_{i+\frac{1}{2},j}+\theta_{i-\frac{1}{2},j}F_{i-\frac{1}{2},j}+\theta_{i,j+\frac{1}{2}}F_{i,j+\frac{1}{2}}+\theta_{i,j-\frac{1}{2}}F_{i,j-\frac{1}{2}}\leq\Gamma^{M}_{i,j}. \tag{5.11}$$

To decouple the inequalities (5.11), for the single node (i,j), we follow those two steps:

1. Identify those positive values out of the four local defined numbers $F_{i-\frac{1}{2},j}$, $F_{i+\frac{1}{2},j}$, $F_{i,j-\frac{1}{2}}$, $F_{i,j+\frac{1}{2}}$.

2. Corresponding to the positive values, collectively, the limiting parameters can be defined. For example, if $F_{i+\frac{1}{2},j}$, $F_{i-\frac{1}{2},j}>0$ and $F_{i,j-\frac{1}{2}}$, $F_{i,j+\frac{1}{2}}\leq 0$, then

$$\begin{cases}\Lambda^{M}_{i-\frac{1}{2},j},\Lambda^{M}_{i+\frac{1}{2},j}=\min(\frac{\Gamma^{M}_{i,j}}{F_{i-\frac{1}{2},j}+F_{i+\frac{1}{2},j}},1),\\ \Lambda^{M}_{i,j-\frac{1}{2}},\Lambda^{M}_{i,j+\frac{1}{2}}=1.\end{cases} \tag{5.12}$$

Similarly, for the minimum value part, let

$$\Gamma^{m}_{i,j}=u_m-(u_{i,j}-\lambda_x(\hat{h}_{i+\frac{1}{2},j}-\hat{h}_{i-\frac{1}{2},j})-\lambda_y(\hat{g}_{i,j+\frac{1}{2}}-\hat{g}_{i,j-\frac{1}{2}}))\leq 0, \tag{5.13}$$

then the coupled inequality (5.6) with (5.5) can be rewritten as

$$\Gamma^{m}_{i,j}\leq\theta_{i+\frac{1}{2},j}F_{i+\frac{1}{2},j}+\theta_{i-\frac{1}{2},j}F_{i-\frac{1}{2},j}+\theta_{i,j+\frac{1}{2}}F_{i,j+\frac{1}{2}}+\theta_{i,j-\frac{1}{2}}F_{i,j-\frac{1}{2}}. \tag{5.14}$$

A similar procedure could be applied as:

1. Identify negative values out of the four locally defined numbers $F_{i-\frac{1}{2},j}$, $F_{i+\frac{1}{2},j}$, $F_{i,j-\frac{1}{2}}$, $F_{i,j+\frac{1}{2}}$.

2. Corresponding to the negative values, collectively, the limiting parameters can be defined. For example, if $F_{i+\frac{1}{2},j}$,$F_{i-\frac{1}{2},j} < 0$ and $F_{i,j-\frac{1}{2}}$, $F_{i,j+\frac{1}{2}} \geq 0$, then

$$\begin{cases} \Lambda^m_{i-\frac{1}{2},j}, \Lambda^m_{i+\frac{1}{2},j} = \min(\frac{\Gamma^m_{i,j}}{F_{i-\frac{1}{2},j}+F_{i+\frac{1}{2},j}}, 1), \\ \Lambda^m_{i,j-\frac{1}{2}}, \Lambda^m_{i,j+\frac{1}{2}} = 1. \end{cases} \tag{5.15}$$

Namely, all high order fluxes which possibly contribute (beyond that by the first order fluxes) to the overshooting or undershooting of the updated value shall be limited by the same scaling. Then the range of the limiting parameters satisfying MPP for a single node (i,j) can be defined by

$$\begin{cases} \Lambda_{L,i,j} = \min(\Lambda^M_{i-\frac{1}{2},j}, \Lambda^m_{i-\frac{1}{2},j}), \\ \Lambda_{R,i,j} = \min(\Lambda^M_{i+\frac{1}{2},j}, \Lambda^m_{i+\frac{1}{2},j}), \\ \Lambda_{U,i,j} = \min(\Lambda^M_{i,j+\frac{1}{2}}, \Lambda^m_{i,j+\frac{1}{2}}), \\ \Lambda_{D,i,j} = \min(\Lambda^M_{i,j-\frac{1}{2}}, \Lambda^m_{i,j-\frac{1}{2}}), \end{cases} \tag{5.16}$$

Considering the limiters from the neighboring nodes, finally we can define the local limiting parameters by

$$\begin{cases} \theta_{i+\frac{1}{2},j} = \min(\Lambda_{R,i,j}, \Lambda_{L,i+1,j}), \\ \theta_{i,j+\frac{1}{2}} = \min(\Lambda_{U,i,j}, \Lambda_{D,i,j+1}), \end{cases} \tag{5.17}$$

which, as in the one-dimensional case, modifies the average integral of the numerical fluxes (symbolically) to provide a sufficient condition for the conservative scheme (5.4) satisfying

maximum principle.

Chapter 6

Numerical simulations [1]

In this chapter, we present numerical tests for the FD RK WENO scheme with parametrized MPP limiter. We use fifth order WENO scheme for spatial approximation and test two types of high order RK method for time discretization. We denote the scheme as "WENO5-TVDRK3" when the third order TVD RK method (4.6) is applied; and "WENO5-RK4" when the following regular fourth order RK method is used. A classical fourth order RK method reads as

$$\begin{aligned} u^{(1)} &= u^n + \frac{1}{2}\Delta t L(u^n), \\ u^{(2)} &= u^n + \frac{1}{2}\Delta t L(u^{(1)}), \\ u^{(3)} &= u^n + \Delta t L(u^{(2)}), \\ u^{n+1} &= u^n + \frac{1}{6}\Delta t \big(L(u^n) + 2L(u^{(1)}) + 2L(u^{(2)}) + L(u^{(3)})\big). \end{aligned} \tag{6.1}$$

[1] The material contained in this chapter has been submitted for publication.

In the compressed form (4.7), the average flux integral is defined as

$$\hat{H}^{rk}_{j+\frac{1}{2}} = \frac{1}{6}(\hat{H}^{(n)}_{j+\frac{1}{2}} - \hat{H}^{D(n)}_{j+\frac{1}{2}}) + \frac{1}{3}(\hat{H}^{(1)}_{j+\frac{1}{2}} - \hat{H}^{D(1)}_{j+\frac{1}{2}}) + \frac{1}{3}(\hat{H}^{(2)}_{j+\frac{1}{2}} - \hat{H}^{D(2)}_{j+\frac{1}{2}}) + \frac{1}{6}(\hat{H}^{(3)}_{j+\frac{1}{2}} - \hat{H}^{D(3)}_{j+\frac{1}{2}}). \tag{6.2}$$

As for the low order monotone scheme, we choose the first order Lax-Friedrichs scheme for the convection part and second order central difference scheme for the diffusion part, unless otherwise stated. Suitable CFL needs to be chosen to ensure that the first order monotone scheme satisfies the maximum principle.

6.1 Basic tests

In this part, we test the performance of the scheme with the general MPP flux limiters to demonstrate that the discrete maximum principle is enforced without compromising the designed order of accuracy. For several problems where exact solutions are unknown, we show the designed scheme satisfactorily preserve maximum principle while producing solutions comparable to what are obtained by regular FD RK WENO scheme.

6.1.1 Standard tests

Example 1 *1D Accuracy Test.*

We test the accuracy of the FD WENO5 scheme for the linear equation

$$u_t + u_x = \varepsilon u_{xx} \tag{6.3}$$

with initial condition $u(x,0) = \sin(x)$ on $[0, 2\pi]$ and periodic boundary conditions, where $\varepsilon = 0.00001$. The exact solution is $e^{-\varepsilon t}\sin(x-t)$. The time step is taken as $\Delta t = \Delta x^{\frac{5}{3}}$ and $\Delta t = \Delta x^{\frac{5}{4}}$ respectively in TVDRK3 and RK4 scheme. For this example, the numerical solution from the regular WENO5-TVDRK3 and WENO5-RK4 schemes do not overshoot or undershoot the theoretical bounds. The results listed in Table 6.1 indicate the MPP flux limiters do not affect the overall accuracy. Clear fifth order accuracy for spatial discretization is observed.

Table 6.1
L^1 and L^∞ error and order for Example 1 with WENO5 scheme at T=1.

	TVD RK3				RK4			
N	L^1error	order	L^∞ error	order	L^1error	order	L^∞ error	order
40	9.62E-06	/	1.98E-05	/	7.60E-06	/	1.59E-05	/
80	3.00E-07	5.01	6.11E-07	5.01	2.26E-07	5.07	4.88E-07	5.02
160	9.39E-09	5.00	1.86E-08	5.04	6.97E-09	5.02	1.47E-08	5.05
320	2.94E-10	5.00	5.22E-10	5.15	2.17E-10	5.01	4.01E-10	5.20
640	9.12E-12	5.01	1.54E-11	5.08	6.73E-12	5.01	1.18E-11	5.09
1280	2.80E-13	5.03	4.64E-13	5.05	2.05E-13	5.04	3.57E-13	5.05

Example 2 *1D MPP Test.*

Consider (6.3) with initial condition

$$u(x,0) = \begin{cases} 1, & |x| > 0.5 \\ -1, & \text{otherwise} \end{cases}$$

on the interval $[-1,1]$. The numerical results in Table 6.2 and 6.3 show that the regular FD RK WENO scheme produces numerical solutions that overshoot and undershoot the bounds of the exact solution. However, with the general parametrized MPP flux limiters,

both of the WENO5-TVDRK3 and WENO5-RK4 schems produce solutions satisfying the maximum principle.

Table 6.2
Maximum and minimum of numerical solutions for Example 2 with WENO5-TVDRK3 scheme at T=1.

	Without Limiter		With Limiter	
N	Umax	Umin	Umax	Umin
40	1.0002063311	-1.0002063311	1.0000000000	-1.0000000000
80	1.0002957746	-1.0002957746	1.0000000000	-1.0000000000
160	1.0004101306	-1.0004101306	1.0000000000	-1.0000000000
320	1.0005575475	-1.0005575475	1.0000000000	-1.0000000000
640	1.0007090407	-1.0007090407	1.0000000000	-1.0000000000
1280	1.0005180275	-1.0005180275	1.0000000000	-1.0000000000

Table 6.3
Maximum and minimum of numerical solutions for Example 2 with WENO5-RK4 scheme at T=1.

	Without Limiter		With Limiter	
N	Umax	Umin	Umax	Umin
40	1.0001347951	-1.0001347951	1.0000000000	-1.0000000000
80	1.0001720631	-1.0001720631	1.0000000000	-1.0000000000
160	1.0002068378	-1.0002068378	1.0000000000	-1.0000000000
320	1.0002029487	-1.0002029487	1.0000000000	-1.0000000000
640	1.0001735970	-1.0001735970	1.0000000000	-1.0000000000
1280	1.0000088943	-1.0000088943	1.0000000000	-1.0000000000

Example 3 *1D Burgers' Equation*

To test the FD RK WENO scheme with MPP flux limiters on the nonlinear problem, we consider the viscous Burgers' equation in one dimension

$$u_t + (u^2)_x = \varepsilon u_{xx} \tag{6.4}$$

with piecewise initial condition

$$u(x,0) = \begin{cases} 2, & |x| < \frac{1}{2} \\ 0, & \text{otherwise on } [-1,1] \end{cases}$$

and periodic boundary conditions, where $\varepsilon = 0.0001$.

The results in both Table 6.4 and 6.5 show that the regular FD RK WENO scheme produce solutions overshooting the upper bounds and undershooting the lower bounds of the initial data. However, when the general parametrized MPP flux limiters are applied, the numerical solutions stay within the desired range.

Table 6.4
Maximum and minimum of numerical solutions for Example 3 with WENO5-TVDRK3 scheme at T=0.05.

	Without Limiter		With Limiter	
N	Umax	Umin	Umax	Umin
40	2.0000418290	-0.0000781962	1.9999976182	0.0000000000
80	2.0000162331	-0.0000859882	2.0000000000	0.0000000000
160	2.0000159331	-0.0001027752	2.0000000000	0.0000000000
320	2.0000250080	-0.0000765844	2.0000000000	0.0000000000
640	2.0000275582	-0.0000430721	2.0000000000	0.0000000000
1280	2.0000130069	-0.0000015064	2.0000000000	0.0000000000

Example 4 *2D Accuracy Test*

We test the MPP FD RK WENO schemes on the two-dimensional linear problems for

Table 6.5
Maximum and minimum of numerical solutions for Example 3 with WENO5-RK4 scheme at T=0.05.

	Without Limiter		With Limiter	
N	Umax	Umin	Umax	Umin
40	1.9999879882	-0.0000770514	1.9999885154	0.0000000000
80	2.0000132842	-0.0000893076	2.0000000000	0.0000000000
160	2.0000136453	-0.0001027328	2.0000000000	0.0000000000
320	2.0000156001	-0.0000757659	2.0000000000	0.0000000000
640	2.0000144806	-0.0000426096	2.0000000000	0.0000000000
1280	2.0000038093	-0.0000015115	2.0000000000	0.0000000000

accuracy. Consider

$$u_t + u_x + u_y = \varepsilon(u_{xx} + u_{yy}) \tag{6.5}$$

with initial condition $u(x,y,0) = \sin(x+y)$ on $[0,2\pi] \times [0,2\pi]$ and periodic boundary conditions, where $\varepsilon = 0.001$. The exact solution is $u(x,y) = e^{-2t\varepsilon}\sin(x+y-2t)$. The time step is taken as $\Delta t = \Delta x^{\frac{5}{3}}$ and $\Delta t = \Delta x^{\frac{5}{4}}$ respectively in TVDRK3 and RK4 scheme. The numerical errors measured in L^1 and L^∞ norm in Table 6.6 clearly indicate that the schemes preserve the designed order of accuracy.

Table 6.6
L^1 and L^∞ error and order for Example 4 with WENO5 scheme at T=0.1.

	TVD RK3				RK4			
N	L^1error	order	L^∞ error	order	L^1error	order	L^∞ error	order
8^2	3.60E-03	/	5.75E-03	/	3.55E-03	/	5.76E-03	/
16^2	2.14E-04	4.07	3.64E-04	3.98	1.85E-04	4.26	3.01E-04	4.26
32^2	9.60E-06	4.48	1.73E-05	4.40	5.00E-06	5.21	9.08E-06	5.05
64^2	4.75E-07	4.34	8.30E-07	4.38	1.44E-07	5.11	3.05E-07	4.90
128^2	1.46E-08	5.02	2.56E-08	5.02	4.31E-09	5.06	9.37E-09	5.02
256^2	4.93E-10	4.89	8.10E-10	4.98	1.32E-10	5.03	2.45E-10	5.26

Example 5 *2D MPP Test*

Consider (6.5) with initial condition

$$u(x,0) = \begin{cases} 1, & (x,y) \in [\frac{\pi}{2}, \frac{3\pi}{2}] \times [\frac{\pi}{2}, \frac{3\pi}{2}] \\ 0, & \text{otherwise} \end{cases}$$

The results in Table 6.7 and 6.8 demonstrate the desired performance of the MPP FD RK WENO scheme that the numerical solutions satisfy the discrete maximum principle for repeatedly refined grids. We also test CPU time for our WENO5-TVDRK3 scheme on this problem. For the scheme without limiter, it took 206 seconds; while for the one with limiter, it took 262 seconds.

Table 6.7
Maximum and minimum of numerical solutions for Example 5 with WENO5-TVDRK3 scheme at T=0.1.

	Without Limiter		With Limiter	
N	Umax	Umin	Umax	Umin
8^2	0.9999415401	-0.0000175795	1.0000000000	0.0000000000
16^2	1.0001780302	-0.0000930712	1.0000000000	0.0000000000
32^2	1.0004407726	-0.0002301740	1.0000000000	0.0000000000
64^2	1.0005165357	-0.0002672254	1.0000000000	0.0000000000
128^2	1.0001754347	-0.0001145699	1.0000000000	0.0000000000
256^2	1.0000857099	-0.0000705472	1.0000000000	0.0000000000

6.1.2 Buckley-Leverett Equation

Example 6 *1D Buckley-Leverett Equation*

Table 6.8
Maximum and minimum of numerical solutions for Example 5 with WENO5-RK4 scheme at T=0.1

	Without Limiter		With Limiter	
N	Umax	Umin	Umax	Umin
8^2	0.9999369261	-0.0000094239	1.0000000000	0.0000000000
16^2	1.0001831478	-0.0000956479	1.0000000000	0.0000000000
32^2	1.0004362470	-0.0002294667	1.0000000000	0.0000000000
64^2	1.0005086147	-0.0002632512	1.0000000000	0.0000000000
128^2	1.0001748274	-0.0001139651	1.0000000000	0.0000000000
256^2	1.0000859656	-0.0000705522	1.0000000000	0.0000000000

We solve the Buckley-Leverett equation

$$u_t + f(u)_x = \varepsilon(\nu(u)u_x)_x \tag{6.6}$$

where the boundary condition $u(0,t) = 1$ and $\varepsilon = 0.01$. The $\nu(u)$ and the initial condition are given as

$$\nu(u) = \begin{cases} 4u(1-u), & 0 \le u \le 1 \\ 0, & \text{otherwise} \end{cases}, \quad u(x,0) = \begin{cases} 1-3x, & 0 \le x < \frac{1}{3} \\ 0, & \frac{1}{3} \le x \le 1 \end{cases} \tag{6.7}$$

with an s-shape $f(u)$:

$$f(u) = \frac{u^2}{u^2 + (1-u)^2}. \tag{6.8}$$

The equation is widely used to model the two-phase flow such as oil and water in a porous medium like soil or rock, where $u(x,t)$ denotes the saturation of water, i.e., the fraction of pore volume occupied by water. Hence, the equation is expected to have a nonnegative solution.

When regular FD RK WENO schemes are used, undershooting is observed in Table 6.9 and 6.10. But after adding the parametrized MPP flux limiters, the undershooting is completely eliminated. The comparison between the regular FD RK WENO scheme and the MPP FD RK WENO shown in Figure 6.1 clearly demonstrates the effect of the parametrized MPP flux limiters.

Table 6.9
Maximum and minimum of numerical solutions for Example 6 with WENO5-TVDRK3 scheme at T=0.2

	Without Limiter		With Limiter	
N	Umax	Umin	Umax	Umin
40	0.9997704140	-0.0014960890	0.9887702120	0.0000000000
80	0.9944686462	-0.0076585662	0.9944686380	0.0000000000
160	0.9970366111	-0.0089641849	0.9970366108	0.0000000000
320	0.9980783981	-0.0273728707	0.9980783981	0.0000000000
640	0.9985103899	-0.0294850154	0.9985103899	0.0000000000
1280	0.9987561434	-0.0199794258	0.9987561434	0.0000000000

Table 6.10
Maximum and minimum of numerical solutions for Example 6 with WENO5-RK4 scheme at T=0.2

	Without Limiter		With Limiter	
N	Umax	Umin	Umax	Umin
40	0.9887372634	-0.0008945524	0.9887704133	0.0000000000
80	0.9944638610	-0.0075621906	0.9944686462	0.0000000000
160	0.9970359567	-0.0092657513	0.9970366111	0.0000000000
320	0.9980783175	-0.0273768885	0.9980783981	0.0000000000
640	0.9985103792	-0.0294859020	0.9985103899	0.0000000000
1280	0.9987561417	-0.0194864853	0.9987561434	0.0000000000

Example 7 *2D Buckley-Leverett Equation*

The two-dimensional Buckley-Leverett equation with gravity in y-direction [13] reads as

$$u_t + f(u)_x + g(u)_y = \varepsilon(u_{xx} + u_{yy}), \tag{6.9}$$

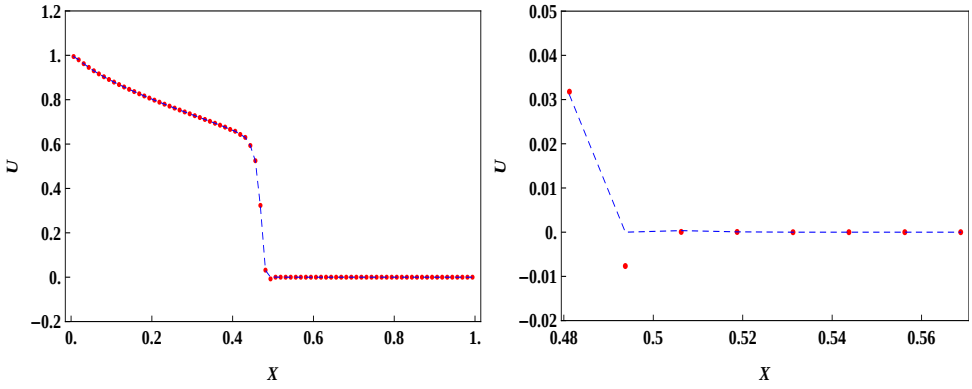

Figure 6.1: Left: Numerical solution for Example 6 with WENO5-TVDRK3 scheme for N=80 when T=0.2. Symbols:Without Limiter; Dashed Line: With Limiter. Right: Zoom in near undershoot.

where

$$f(u) = \frac{u^2}{u^2 + (1-u)^2}, \quad g(u) = f(u)(1 - 5(1-u)^2). \tag{6.10}$$

For $\varepsilon = 0.01$ and periodic boundary condition we compute the problem with the initial condition

$$u(x,y,0) = \begin{cases} 1, & x^2 + y^2 < 0.5 \\ 0, & \text{otherwise.} \end{cases} \tag{6.11}$$

Quantitatively, we can observe the undershooting of the lower bound of the exact solution when regular FD RK WENO method is used. As we expect, those undershoots are completely eliminated by applying the parametrized MPP flux limiters to the regular FD RK WENO method, as can be seen in Table 6.11 and 6.12. The contour plot in Figure 6.2 shows that the overall solution is comparable to what was obtained by regular FD RK

WENO method.

Table 6.11
Maximum and minimum of numerical solutions for Example 7 with WENO5-TVDRK3 scheme at T=0.5.

	Without Limiter		With Limiter	
N	Umax	Umin	Umax	Umin
8^2	0.6888730009	-0.0002020615	0.6781934107	0.0000000000
16^2	0.9323237340	-0.0107944114	0.9319601262	0.0000000000
32^2	0.9531022099	-0.0011386839	0.9531020193	0.0000000000
64^2	0.9779664782	-0.0000297787	0.9779676116	0.0000000000
128^2	0.9888119638	-0.0000065591	0.9888103124	0.0000000000
256^2	0.9933051368	0.0000000000	0.9933033014	0.0000000000

Table 6.12
Maximum and minimum of numerical solutions for Example 7 with WENO5-RK4 scheme at T=0.5.

	Without Limiter		With Limiter	
N	Umax	Umin	Umax	Umin
8	0.6888305800	-0.0001950800	0.6807012673	0.0000000000
16	0.9323720974	-0.0108174288	0.9320612550	0.0000000000
32	0.9531092030	-0.0011388357	0.9531053582	0.0000000000
64	0.9779660833	-0.0000297796	0.9779676880	0.0000000000
128	0.9888118380	-0.0000065589	0.9888103278	0.000000000
256	0.9933050977	0.0000000000	0.9933033035	0.0000000000

6.1.3 Porous Medium Equation

Example 8 *1D MPP Test*

In this example, we test the scheme on the one-dimensional porous medium equation

$$u_t = (u^m)_{xx}, \quad m > 1, \tag{6.12}$$

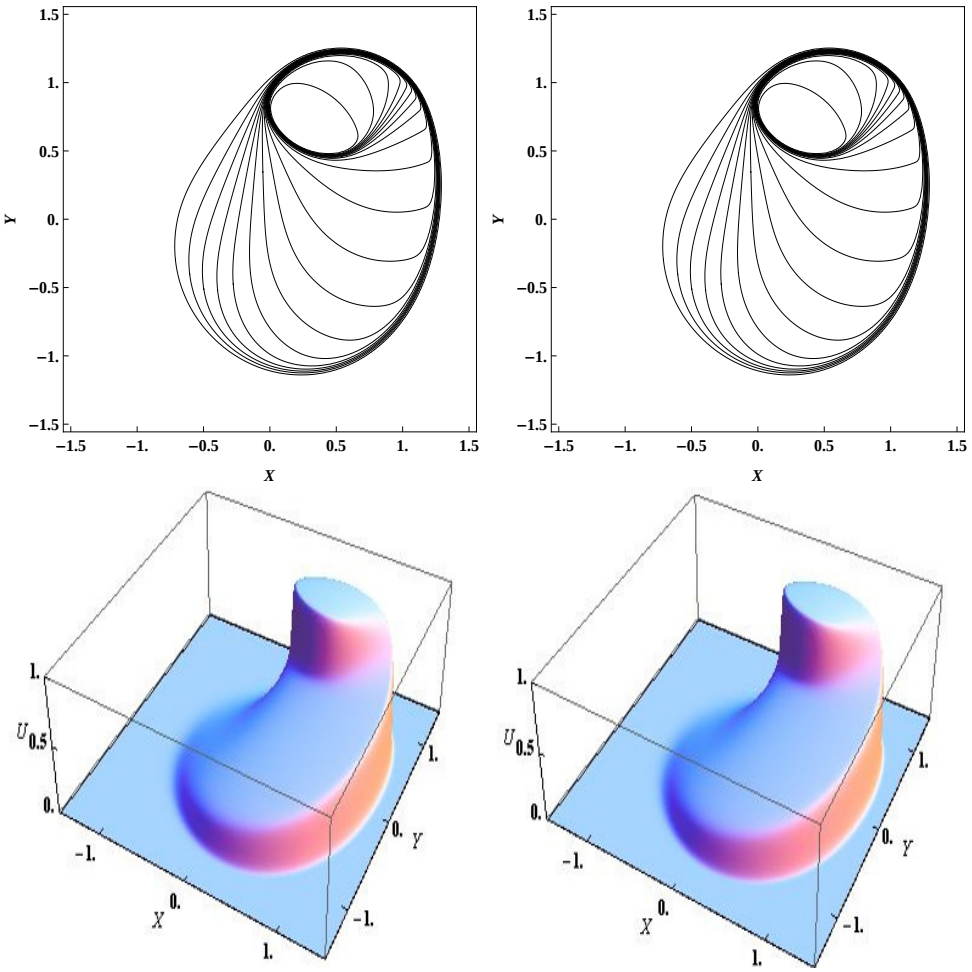

Figure 6.2: Numerical solutions for Example 7 with WENO5-TVDRK3 scheme at T=0.5 on a 256×256 mesh. Left:Without Limiter; Right: With Limiter.

which describes the flow of an ideal gas through a homogeneous porous medium (soil or foam, for example) [21]. The function of interest $u(x,t)$ is the density of the flow, which, physically speaking, should only have nonnegative values. Since there is no convection in the equation, we test the general MPP flux limiters applied to the 6th order central difference scheme, denoted as CD6, for the Barenblatt solution

$$B_m(x,t) = t^{-k}[(1 - \frac{k(m-1)}{2m}\frac{|x|^2}{t^{2k}})_+]^{1/(m-1)}, \tag{6.13}$$

where $u_+ = \max(u,0)$ and $k = (m+1)^{-1}$. The initial condition is the Barenblatt solution at

t=1 and the boundary condition is zero for both ends. For a fixed grid $N = 80$, we compute the solution for different m's. For regular FD RK WENO methods, negative values emerge in all the computations and, again, the general parametrized MPP flux limiters remedied the negative values in a conservative way, see Table 6.13 and Table 6.14. The corresponding numerical solutions are also plotted in Figure 6.3. The solutions obtained from WENO schemes with or without MPP flux limiters are comparable overall.

Table 6.13
Maximum and minimum of the numerical solutions for Example 8 with CD6-TVDRK3 scheme at T=2.

N=80	Without Limiter		With Limiter	
m	Umax	Umin	Umax	Umin
2	0.7934728773	-0.0009481257	0.7934703792	0.0000000000
3	0.8407913334	-0.0044816384	0.8407704961	0.0000000000
5	0.8910119047	-0.0002067887	0.8909759011	0.0000000000
8	0.9257011131	-0.0295555446	0.9256537064	0.0000000000

Table 6.14
Maximum and minimum of the numerical solutions for Example 8 with CD6-RK4 scheme at T=2.

N=80	Without Limiter		With Limiter	
m	Umax	Umin	Umax	Umin
2	0.7934728778	-0.0009481110	0.7934703799	0.0000000000
3	0.8407913334	-0.0044816384	0.8407704945	0.0000000000
5	0.8910119047	-0.0002067893	0.8909759018	0.0000000000
8	0.9257011131	-0.0295555445	0.9256537059	0.0000000000

Example 9 *2D MPP Test for porous medium equation*

We compute the solution to the two-dimensional porous medium equation

$$u_t = (u^2)_{xx} + (u^2)_{yy} \tag{6.14}$$

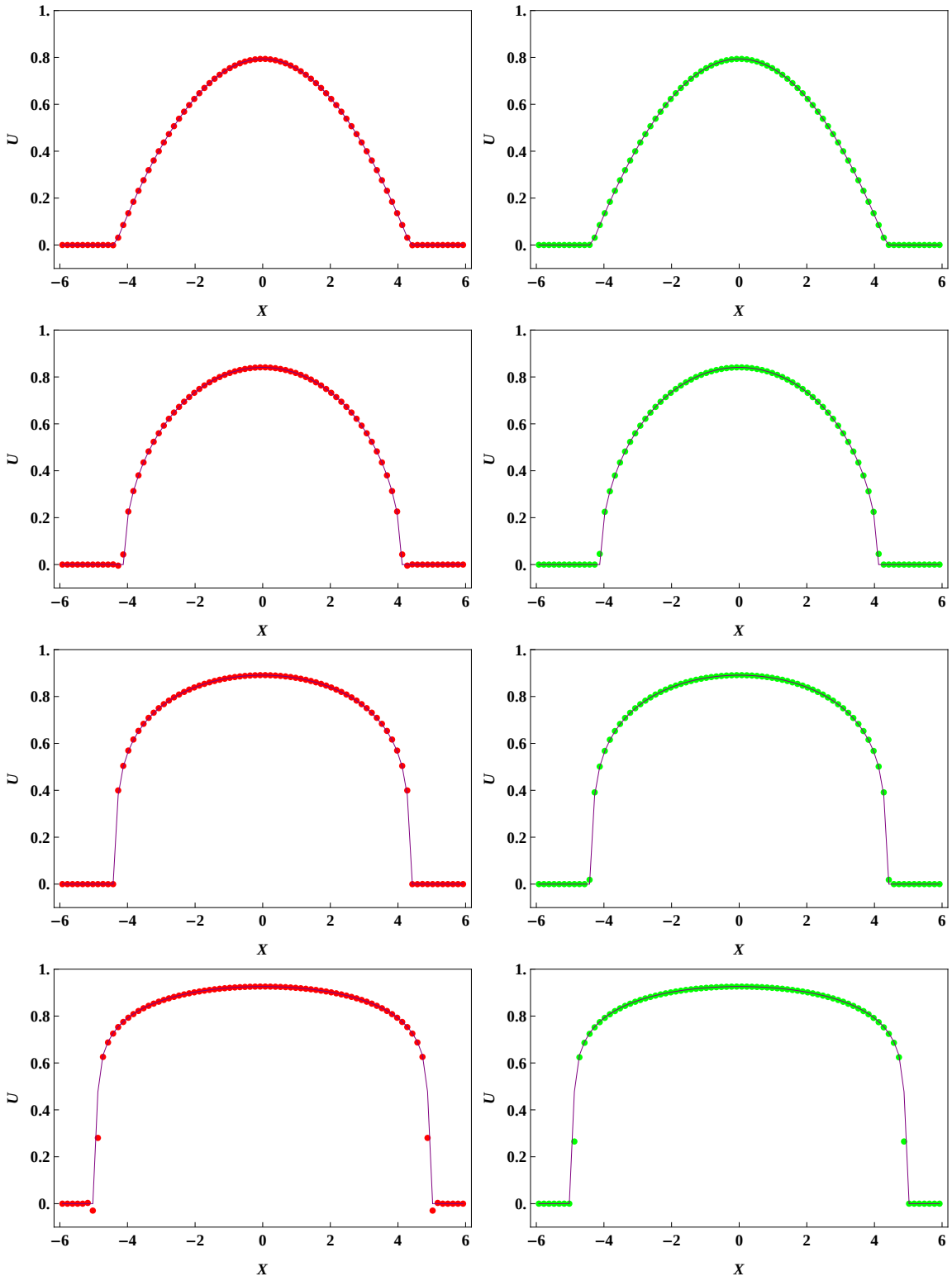

Figure 6.3: Top to bottom: m=2, 3, 5, 8; Solid Line: exact solution; Symbol: numerical solution for Example 8 with CD6-TVDRK3 scheme; Left: Without Limiter; Right: With Limiter; T=2.

with the initial condition

$$u(x,y,0) = \begin{cases} 1, & (x,y) \in [-\frac{1}{2},\frac{1}{2}] \times [-\frac{1}{2},\frac{1}{2}], \\ 0, & \text{otherwise on } [-1,1] \times [-1,1]. \end{cases} \tag{6.15}$$

The boundary conditions are periodic. Numerical results listed in Table 6.15 and 6.16 include the maximum and minimum of the numerical solutions at T=0.005 for sixth order central difference scheme. The numerical solution of the regular central difference experiences undershooting and overshooting. With the general MPP flux limiters, the undershoots and overshoots are eliminated in the repeatedly refined numerical study. The overall performance of the scheme with MPP limiters is compared with the regular central difference scheme in Figure 6.4. The result is comparable to what is obtained by the MPP finite volume method [35, 34]. It is safe to say that the modified scheme performs satisfactorily.

Table 6.15
Maximum and minimum of the numerical solutions for Example 9 with CD6-TVDRK3 scheme at T=0.005.

	Without Limiter		With Limiter	
Mesh	Umax	Umin	Umax	Umin
8^2	1.0004978920	-0.0088618987	1.0000000000	0.0000000000
16^2	0.9996875340	-0.0164741747	0.9994583313	0.0000000000
32^2	0.9994788981	-0.0100280290	0.9994761086	0.0000000000
64^2	0.9995111399	-0.0047699036	0.9995083661	0.0000000000
128^2	0.9995214235	-0.0024365666	0.9995195806	0.0000000000
256^2	0.9995240567	-0.0011828286	0.9995232196	0.0000000000

Table 6.16
Maximum and minimum of the numerical solutions for Example 9 with CD6-RK4 scheme at T=0.005

	Without Limiter		With Limiter	
Mesh	Umax	Umin	Umax	Umin
8^2	1.0000080795	-0.0088714497	1.0000000000	0.0000000000
16^2	0.9997246554	-0.0164826719	0.9994691425	0.0000000000
32^2	0.9994782553	-0.0100280542	0.9994711759	0.0000000000
64^2	0.9995110279	-0.0047699241	0.9995076405	0.0000000000
128^2	0.9995214082	-0.0024365595	0.9995194547	0.0000000000
256^2	0.9995240550	-0.0011828263	0.9995231952	0.0000000000

6.2 Incompressible flow

In this section, we will test the parametrized MPP flux limiters on several incompressible flow problems. Through those examples, we would like to show that FD RK WENO scheme maintains designed high order accuracy when the solution is smooth. Maximum principle is satisfied, which provides a weak stability when computing the incompressible Navier-Stokes equation in the vorticity-stream function formulation.

The solution to the incompressible flow problem satisfies the maximum principle in theory due to the divergence-free property of the velocity field, namely $\nabla \cdot \mathbf{u} = 0$. However numerically, the discretized divergence-free property has to be delicately built into the scheme to ensure that the numerical scheme also preserves the maximum principle. For this part of the numerical tests, we apply the first order monotone scheme designed in [32] for the pure convection term of the incompressible flow. For the diffusion term, we still use second-order central difference as our lower order scheme.

Example 10 *Rotation with viscosity*

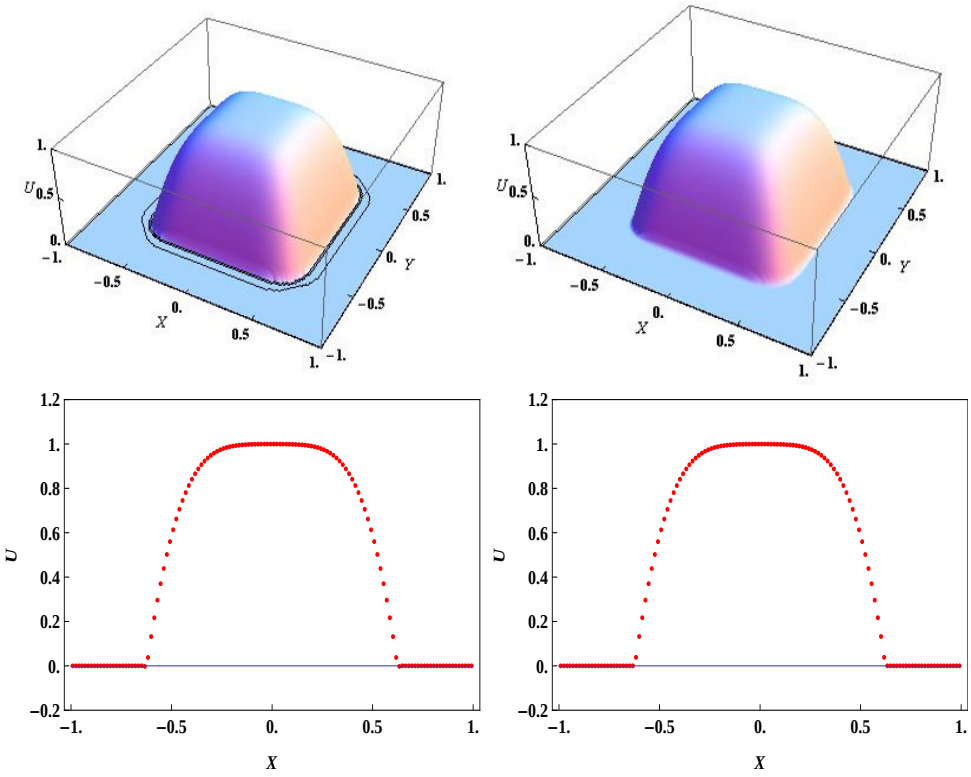

Figure 6.4: Example 9 with CD6-TVDRK3 scheme at T=0.005 on a 64×64 grid; Top: surface; Bottom: cut along with $y = \Delta y$; Left:Without Limiter; Right: With Limiter.

The first incompressible flow involves a body rotation with viscosity

$$u_t - (yu)_x + (xu)_y = \frac{1}{Re}(u_{xx} + u_{yy}), \quad (x,y) \in [-\pi,\pi] \times [-\pi,\pi] \tag{6.16}$$

with the periodic boundary conditions and $Re = 100$. The initial condition includes a slotted disk, a cone, and a smooth hump as shown in Figure 6.5. For repeatedly refined grids, we can observe both overshooting and undershooting in Table 6.17 and 6.18. Meanwhile, the overshooting and undershooting disappear when the parametrized MPP flux limiters are applied.

Example 11 *Swirling deformation flow with viscosity*

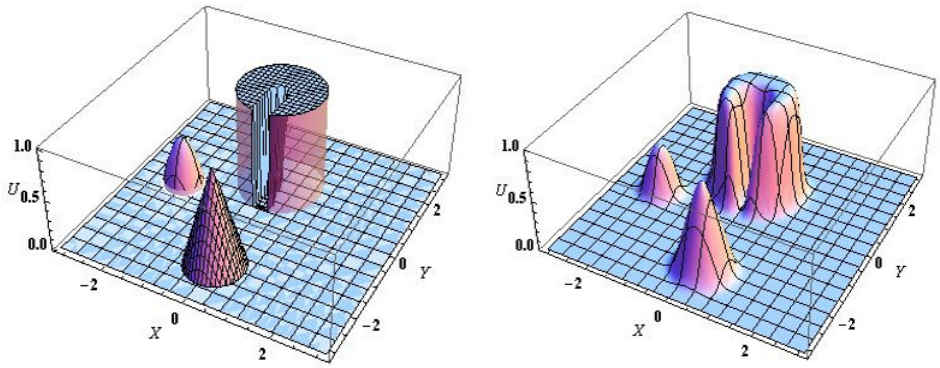

Figure 6.5: Plots for Example 10. Left: Initial profile; Right: Numerical solution from WENO5-TVDRK3 scheme with limiter at T=0.1.

Table 6.17
Maximum and minimum of numerical solutions for Example 10 with WENO5-TVDRK3 scheme at T=0.1

	Without Limiter		With Limiter	
Mesh	Umax	Umin	Umax	Umin
8^2	0.8575998565	-0.0009106636	0.8576177974	0.0000000000
16^2	0.8667285539	-0.0001892116	0.8667301366	0.0000000000
32^2	1.0190769175	-0.0008895879	1.0000000000	0.0000000000
64^2	1.0012162433	-0.0146238716	1.0000000000	0.0000000000
128^2	1.0000417179	-0.0000282575	1.0000000000	0.0000000000
256^2	1.0000047098	-0.0000052679	1.0000000000	0.0000000000

Table 6.18
Maximum and minimum of numerical solutions for Example 10 with WENO5-RK4 scheme at T=0.1

	Without Limiter		With Limiter	
Mesh	Umax	Umin	Umax	Umin
8^2	0.8576698441	-0.0009253533	0.8576864150	0.0000000000
16^2	0.8673045790	-0.0001914213	0.8673050582	0.0000000000
32^2	1.0192176257	-0.0008096144	1.0000000000	0.0000000000
64^2	1.0011928905	-0.0146744676	1.0000000000	0.0000000000
128^2	1.0000416644	-0.0000282932	1.0000000000	0.0000000000
256^2	1.0000047057	-0.0000052653	1.0000000000	0.0000000000

Table 6.19
Maximum and minimum of numerical solutions for Example 11 with WENO5-TVDRK3 scheme at T=0.1

	Without Limiter		With Limiter	
Mesh	Umax	Umin	Umax	Umin
8^2	0.8846714971	-0.0011482996	0.8849087663	0.0000000000
16^2	0.8485304161	-0.0004016319	0.8492079009	0.0000000000
32^2	1.0212155556	-0.0000585725	1.0000000000	0.0000000000
64^2	1.0015195630	-0.0000483656	1.0000000000	0.0000000000
128^2	1.0001754286	-0.0000258516	1.0000000000	0.0000000000
256^2	1.0000109740	-0.0000027825	1.0000000000	0.0000000000

We consider the swirling deformation flow with viscosity

$$u_t - (\cos^2(\frac{x}{2})\sin(y)g(t)u)_x + (\sin(x)\cos^2(\frac{y}{2})g(t)u)_y = \frac{1}{Re}(u_{xx}+u_{yy}), \tag{6.17}$$

where $(x,y) \in [-\pi,\pi]\times[-\pi,\pi]$, $Re = 100$ and $g(t) = \cos(\pi t/T)\pi$. We assume periodic boundary conditions for simplicity. The initial condition is the same as shown in Figure 6.5. The results in Table 6.19 and 6.20 indicate that the parametrized MPP flux limiters satisfactorily correct the undershooting and overshooting by the original FD RK WENO scheme. The modified scheme produces similar resolution of the original FD RK WENO scheme overall as shown in Figure 6.6.

Table 6.20
Maximum and minimum of numerical solutions for Example 11 with WENO5-RK4 scheme at T=0.1

	Without Limiter		With Limiter	
Mesh	Umax	Umin	Umax	Umin
8^2	0.8839470475	-0.0011448488	0.8839449938	0.0000000000
16^2	0.8468012150	-0.0004057060	0.8468042224	0.0000000000
32^2	1.0217113832	-0.0000579336	1.0000000000	0.0000000000
64^2	1.0015292438	-0.0000484112	1.0000000000	0.0000000000
128^2	1.0001741041	-0.0000258520	1.0000000000	0.0000000000
256^2	1.0000108690	-0.0000027820	1.0000000000	0.0000000000

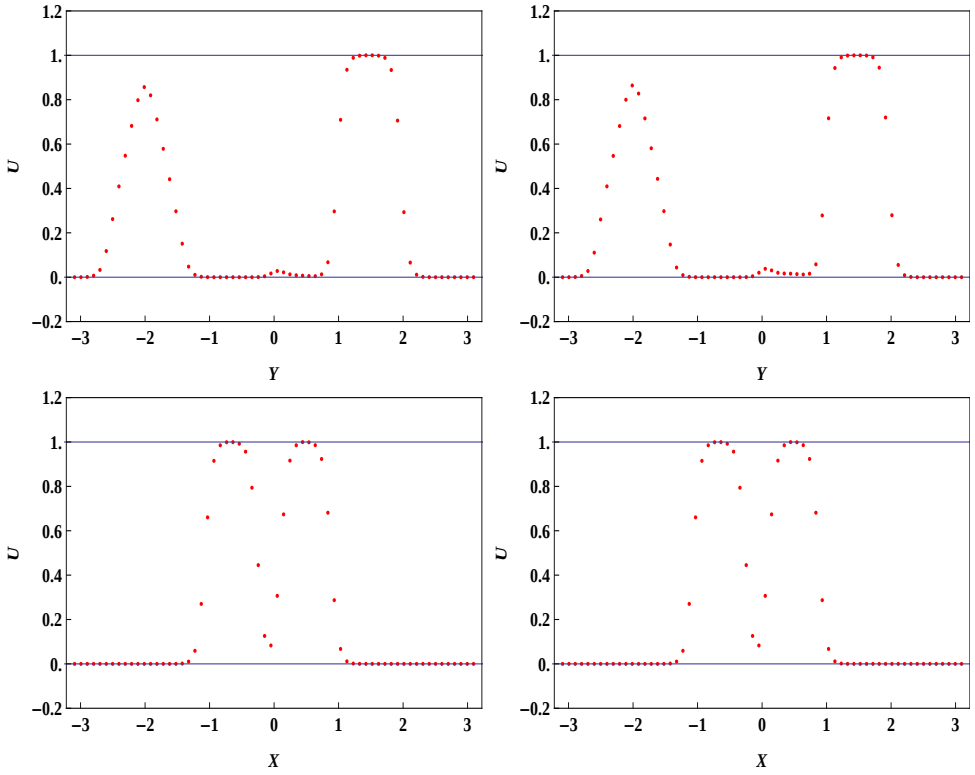

Figure 6.6: Numerical solutions for Example 11 with WENO5-TVDRK3 scheme at T=0.1 on a 64×64 mesh. Cut along x=$-\pi + 32\Delta x$ and y=$-\pi + 40\Delta y$ from top to bottom, respectively. Left: Without Limiter; Right: With Limiter.

Example 12 *Accuracy Test*

The Navier-Stokes equation in the vorticity-stream function formulation reads as

$$\begin{aligned} \omega_t + (u\omega)_x + (v\omega)_y &= \frac{1}{Re}\Delta\omega, \\ \Delta\psi = \omega, \langle u, v\rangle &= \langle -\psi_y, \psi_x\rangle, \\ \omega(x,y,0) &= \omega_0(x,y), \end{aligned} \tag{6.18}$$

with periodic boundary conditions, where $Re = 100$ and $(x,y) \in [0,2\pi] \times [0,2\pi]$. The exact

Table 6.21
L^1 and L^∞ error and order for Example 12 with WENO5 Scheme solving (6.18), at T=0.1

	TVD RK3				RK4			
N	L^1error	order	L^∞ error	order	L^1error	order	L^∞ error	order
8	1.18E-02	/	1.85E-02	/	1.18E-01	/	1.85E-02	/
16	1.86E-03	2.67	6.02E-03	1.62	1.86E-03	2.67	6.02E-03	1.62
32	1.24E-04	3.91	1.05E-03	2.52	1.24E-04	3.91	1.05E-03	2.52
64	4.34E-06	4.84	5.03E-05	4.38	4.34E-06	4.84	5.03E-05	4.38
128	1.39E-07	4.97	2.58E-06	4.29	1.39E-07	4.97	2.58E-06	4.29
256	3.19E-09	5.45	6.23E-08	5.38	3.19E-09	5.45	6.23E-08	5.37

solution is $u(x,y) = -2\sin(x)\sin(y)\exp(-2t/Re)$. We choose time steps as $\Delta t = \Delta x^{\frac{5}{3}}$ and $\Delta t = \Delta x^{\frac{5}{4}}$ respectively in TVDRK3 and RK4 scheme. Through this test, we want to show when the parametrized MPP flux limiters are applied to the FD RK WENO methods solving (6.18), the designed high order accuracy is not affected as can be confirmed by the results listed in Table 6.21.

Example 13 *The Vortex Patch Problem*

We consider the Navier-Stokes equations (6.18) with $Re = 100$ in $[0,2\pi]\times[0,2\pi]$ with the periodic boundary conditions. The initial condition is given as

$$\omega(x,y,0) = \begin{cases} -1, & \frac{\pi}{2} \le x \le \frac{3\pi}{2}, \frac{\pi}{4} \le y \le \frac{3\pi}{4}, \\ 1, & \frac{\pi}{2} \le x \le \frac{3\pi}{2}, \frac{5\pi}{4} \le y \le \frac{7\pi}{4}, \\ 0, & \text{otherwise.} \end{cases} \tag{6.19}$$

The results in Table 6.22 and 6.23 demonstrate the effectiveness of the parametrized flux limiters. The graph in Figure 6.7 shows the results obtained by MPP FD RK WENO

method are comparable to the ones obtained by regular FD RK WENO method.

Table 6.22
Maximum and minimum of the numerical solutions for Example 13 with WENO5-TVDRK3 scheme at T=0.1

	Without Limiter		With Limiter	
Mesh	Umax	Umin	Umax	Umin
8^2	0.9839826621	-0.9839826621	0.9911051547	-0.9909343728
16^2	1.0009658017	-1.0009658017	0.9999121604	-0.9999361764
32^2	1.0006488464	-1.0006488464	0.9999975219	-0.9999983288
64^2	1.0006244343	-1.0006244343	0.9999993276	-0.9999996374
128^2	1.0003261172	-1.0003261172	0.9999997996	-0.9999998514
256^2	1.0000000013	-1.0000000013	0.9999999304	-0.9999999428

Table 6.23
Maximum and minimum of the numerical solutions for Example 13 with WENO5-RK4 scheme at T=0.1

	Without Limiter		With Limiter	
Mesh	Umax	Umin	Umax	Umin
8^2	0.9839838165	-0.9839838165	0.9911052863	-0.9909343858
16^2	1.0009908691	-1.0009908691	0.9999121624	-0.9999121624
32^2	1.0007598682	-1.0007598682	0.9999975219	-0.9999983288
64^2	1.0006307544	-1.0006307544	0.9999993276	-0.9999996374
128^2	1.0003262785	-1.0003262785	0.9999997996	-0.9999998514
256^2	1.0000000013	-1.0000000013	0.9999999304	-0.9999999428

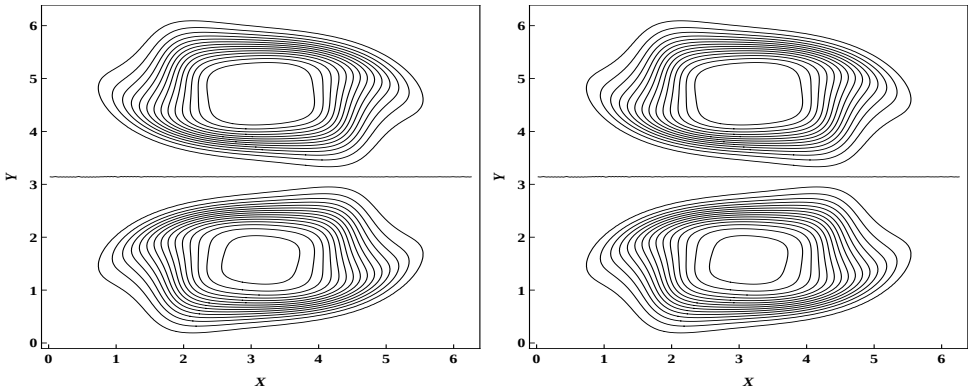

Figure 6.7: Contour plots of numerical solutions for Example 13 with WENO5-TVDRK3 scheme on a 128×128 mesh at T=5. Left: Without Limiter; Right: With Limiter.

Chapter 7

Conclusions and future work

The theme of this thesis is to explore MPP high order schemes solving convection-dominated diffusion equations. We briefly introduced ENO/WENO reconstruction technique with FD and FV method, reviewed a MPP high order FV scheme with a linear scaling limiter, and then proposed a novel parametrized MPP flux limiting high order FD RK WENO framework, where we generalized the MPP limiter designed for high order numerical schemes solving hyperbolic conservation laws to solving convection-dominated diffusion equations with a full high order finite difference RK WENO framework. The proposed method has several advantages. First, it could be conveniently implemented with only requirement of conservative discretization of both convection and diffusion term, which is a natural and standard procedure. Second, the restriction on time step is less demanding. For 1D general nonlinear convection-dominated diffusion equation, analysis based on Taylor expansion in both temporal and spatial direction with the help of PDE is given to justify the maintenance of third order of accuracy, when the MPP limiter is applied to a third order finite difference scheme with an appropriate choice of low order monotone flux. Standard numerical tests and further application to incompressible flows problems are presented to show the effectiveness of

the method with higher order finite difference scheme. The simulations are conducted in both 1D and 2D cases.

A more generalized proof to higher order scheme will be investigated as our future project. We also hope to provide a full theoretical analysis for relevant 2D problems. Furthermore, since it seems pretty straight forward to apply the new parametrized MPP flux limiters to the regular high order finite volume WENO scheme, it's worthy pursuing such scheme solving convection-dominated diffusion problems in the future.

References

[1] Grigory I Barenblatt. On self-similar motions of a compressible fluid in a porous medium. *Akad. Nauk SSSR. Prikl. Mat. Meh*, 16(6):79–6, 1952.

[2] Istvan Farago and Robert Horvath. Discrete maximum principle and adequate discretizations of linear parabolic problems. *SIAM Journal on Scientific Computing*, 28(6):2313–2336, 2006.

[3] István Faragó, János Karátson, and Sergey Korotov. Discrete maximum principles for nonlinear parabolic pde systems. *IMA Journal of Numerical Analysis*, 32(4):1541–1573, 2012.

[4] Emad Fatemi, Joseph Jerome, and Stanley Osher. Solution of the hydrodynamic device model using high-order nonoscillatory shock capturing algorithms. *Computer-Aided Design of Integrated Circuits and Systems, IEEE Transactions on*, 10(2):232–244, 1991.

[5] H Fujii. Some remarks on finite element analysis of time-dependent field problems. *Theory and practice in finite element structural analysis*, pages 91–106, 1973.

[6] Sigal Gottlieb, David I Ketcheson, and Chi-Wang Shu. High order strong stability preserving time discretizations. *Journal of Scientific Computing*, 38(3):251–289, 2009.

[7] Sigal Gottlieb, Chi-Wang Shu, and Eitan Tadmor. Strong stability-preserving high-order time discretization methods. *SIAM review*, 43(1):89–112, 2001.

[8] Ami Harten, Bjorn Engquist, Stanley Osher, and Sukumar R Chakravarthy. Uniformly high order accurate essentially non-oscillatory schemes, iii. *Journal of Computational Physics*, 71(2):231–303, 1987.

[9] Ami Harten and Stanley Osher. Uniformly high-order accurate non-oscillatory schemes, i. *SIAM Journal on Numerical Analysis*, 24(2):279–309, 1987.

[10] Ami Harten, Stanley Osher, Björn Engquist, and Sukumar R Chakravarthy. Some results on uniformly high-order accurate essentially nonoscillatory schemes. *Applied Numerical Mathematics*, 2(3):347–377, 1986.

[11] Guang-Shan Jiang and Chi-Wang Shu. Efficient implementation of weighted eno schemes. Technical report, 1996.

[12] Yi Jiang and Zhengfu Xu. Parametrized maximum principle preserving limiter for finite difference weno schemes solving convection-dominated diffusion equations. *Submitted to SIAM Journal on Scientific Computing*.

[13] Alexander Kurganov and Eitan Tadmor. New high-resolution central schemes for nonlinear conservation laws and convection–diffusion equations. *Journal of Computational Physics*, 160(1):241–282, 2000.

[14] Doron Levy. A stable semi-discrete central scheme for the two-dimensional incompressible euler equations. *IMA journal of numerical analysis*, 25(3):507–522, 2005.

[15] Chao Liang and Zhengfu Xu. Parametrized maximum principle preserving flux limiters for high order schemes solving multi-dimensional scalar hyperbolic conservation laws. *Journal of Scientific Computing*, pages 1–20, 2013.

[16] Xu-Dong Liu and Stanley Osher. Nonoscillatory high order accurate self-similar maximum principle satisfying shock capturing schemes i. *SIAM Journal on Numerical Analysis*, 33(2):760–779, 1996.

[17] Xu-Dong Liu, Stanley Osher, and Tony Chan. Weighted essentially non-oscillatory schemes. *Journal of computational physics*, 115(1):200–212, 1994.

[18] Yuan-yuan Liu, Chi-wang Shu, and Meng-ping Zhang. On the positivity of linear weights in weno approximations. *Acta Mathematicae Applicatae Sinica, English Series*, 25(3):503–538, 2009.

[19] Yuanyuan Liu, Chi-Wang Shu, and Mengping Zhang. High order finite difference weno schemes for nonlinear degenerate parabolic equations. *SIAM Journal on Scientific Computing*, 33(2):939–965, 2011.

[20] Akira Mizukami and Thomas JR Hughes. A petrov-galerkin finite element method for convection-dominated flows: an accurate upwinding technique for satisfying the maximum principle. *Computer Methods in Applied Mechanics and Engineering*, 50(2):181–193, 1985.

[21] M Muskat. The flow of homogeneous fluids through porous media. (1937). *Mac Graw Hill, New York*.

[22] Benoit Perthame and Chi-Wang Shu. On positivity preserving finite volume schemes for euler equations. *Numerische Mathematik*, 73(1):119–130, 1996.

[23] Jing Shi, Changqing Hu, and Chi-Wang Shu. A technique of treating negative weights in weno schemes. *Journal of Computational Physics*, 175(1):108–127, 2002.

[24] Chi-Wang Shu. Total-variation-diminishing time discretizations. *SIAM Journal on Scientific and Statistical Computing*, 9(6):1073–1084, 1988.

[25] Chi-Wang Shu. Numerical experiments on the accuracy of eno and modified eno schemes. *Journal of Scientific Computing*, 5(2):127–149, 1990.

[26] Chi-Wang Shu. *Essentially non-oscillatory and weighted essentially non-oscillatory schemes for hyperbolic conservation laws*. Springer, 1998.

[27] Chi-Wang Shu. High order weighted essentially nonoscillatory schemes for convection dominated problems. *SIAM review*, 51(1):82–126, 2009.

[28] Chi-Wang Shu and Stanley Osher. Efficient implementation of essentially non-oscillatory shock-capturing schemes. *Journal of Computational Physics*, 77(2):439–471, 1988.

[29] Chi-Wang Shu and Stanley Osher. Efficient implementation of essentially non-oscillatory shock-capturing schemes, ii. *Journal of Computational Physics*, 83(1):32–78, 1989.

[30] Tomáš Vejchodskỳ, Sergey Korotov, and Antti Hannukainen. Discrete maximum principle for parabolic problems solved by prismatic finite elements. *Mathematics and Computers in Simulation*, 80(8):1758–1770, 2010.

[31] Yulong Xing, Xiangxiong Zhang, and Chi-Wang Shu. Positivity-preserving high order well-balanced discontinuous galerkin methods for the shallow water equations. *Advances in Water Resources*, 33(12):1476–1493, 2010.

[32] Tao Xiong, Jing-Mei Qiu, and Zhengfu Xu. A parametrized maximum principle preserving flux limiter for finite difference rk-weno schemes with applications in incompressible flows. *Accepted by Journal of Computational Physics for publication.*

[33] Z Xu. Parametrized maximum principle preserving flux limiters for high order scheme solving hyperbolic conservation laws: one-dimensional scalar problem. *Accepted by Mathematics of Computation for publication*.

[34] Qiang Zhang and Zi-Long Wu. Numerical simulation for porous medium equation by local discontinuous galerkin finite element method. *Journal of Scientific Computing*, 38(2):127–148, 2009.

[35] Xiangxiong Zhang, Yuanyuan Liu, and Chi-Wang Shu. Maximum-principle-satisfying high order finite volume weighted essentially nonoscillatory schemes for convection-diffusion equations. *SIAM Journal on Scientific Computing*, 34(2):A627–A658, 2012.

[36] Xiangxiong Zhang and Chi-Wang Shu. On maximum-principle-satisfying high order schemes for scalar conservation laws. *Journal of Computational Physics*, 229(9):3091–3120, 2010.

[37] Xiangxiong Zhang and Chi-Wang Shu. On positivity-preserving high order discontinuous galerkin schemes for compressible euler equations on rectangular meshes. *Journal of Computational Physics*, 229(23):8918–8934, 2010.

[38] Xiangxiong Zhang and Chi-Wang Shu. Maximum-principle-satisfying and positivity-preserving high-order schemes for conservation laws: survey and new developments. *Proceedings of the Royal Society A: Mathematical, Physical and Engineering Science*, 467(2134):2752–2776, 2011.

[39] Xiangxiong Zhang and Chi-Wang Shu. Positivity-preserving high order discontinuous galerkin schemes for compressible euler equations with source terms. *Journal of Computational Physics*, 230(4):1238–1248, 2011.

[40] Xiangxiong Zhang, Yinhua Xia, and Chi-Wang Shu. Maximum-principle-satisfying and positivity-preserving high order discontinuous galerkin schemes for conservation laws on triangular meshes. *Journal of Scientific Computing*, 50(1):29–62, 2012.

[41] Yifan Zhang, Xiangxiong Zhang, and Chi-Wang Shu. Maximum-principle-satisfying second order discontinuous galerkin schemes for convection-diffusion equations on triangular meshes. *Journal of Computational Physics*, 234:295–316, 2013.